Modeling and simulation of particle doped composites for electromagnetic applications

By

Bhavesh Patel

A dissertation submitted in partial satisfaction of the

requirements for the degree of

Doctor of Philosophy

in

Engineering - Mechanical Engineering

in the

Graduate Division

of the

University of California, Berkeley

Committee in charge:

Professor Tarek I. Zohdi, Chair
Professor George C. Johnson
Professor Per-Olof Persson

Spring 2015

Modeling and simulation of particle doped composites for electromagnetic applications

Abstract

Modeling and simulation of particle doped composites for electromagnetic applications

by

Bhavesh Patel

Doctor of Philosophy in Engineering - Mechanical Engineering

University of California, Berkeley

Professor Tarek I. Zohdi, Chair

Most modern electromagnetic devices consist of dielectric and magnetic particulate composites, which are designed with specific properties for delivering optimal performance. Predicting the effective electric permittivity and effective magnetic permeability of the envisioned composite is of great importance in validating the design for such applications. Analytical bounds to estimate these effective properties can be found in literature. However, they often yield large solution ranges and do not account for the microstructure of the composite. We present here a numerical method to estimate these effective electromagnetic properties for any given composite microstructure. It consists of solving Maxwell's equations numerically using a particular Finite Difference Time Domain (FTDT) method, known as Yee's scheme, over a representative volume element of the composite of interest. It allows capturing its electromagnetic response, and subsequently computing its effective electromagnetic properties. Results obtained with this method show good agreement with analytical bounds and experimental data. We also observe more accurate estimations than analytical bounds. The method is then used to assess thermal influence on these effective electromagnetic properties. A numerical design tool, that combines the optimization technique known as genetic algorithm with the proposed numerical method for estimating effective electromagnetic properties, is also presented. It allows determining the required composition and microstructure parameters for a particle doped composite in order to achieve the desired effective electromagnetic properties.

To my father Vinod, my mother Jayashree, my sister Dharati, my brother Mitesh, and my wife Dhara

Contents

List of Figures

List of Tables

Acknowledgments

I would like to express my deepest appreciation to my advisor Professor Tarek Zohdi. He welcomed me into his lab and provided me with the guidance I required. I am extremely thankful to him.

I would like to thank my committee members, Professor George Johnson and Professor Per-Olof Persson, for their feedbacks and advices during my course work and throughout my progress on this dissertation.

I wish to express my sincere gratitude to Professor John Strain for the many insightful discussions and suggestions.

I would also like to thank my labmates at the Computational Materials Research Lab for their constant help and support.

Finally, I gratefully acknowledge King Abdullah University of Science and Technology (KAUST), the funding source that made this dissertation possible.

Chapter 1

Introduction

Composite materials are widely used in a variety of fields [24] mainly due to the flexibility in properties they provide. Indeed, by appropriately choosing constituents and mixture parameters, such as materials volume fraction or filler size, it is possible to develop a material with overall properties adapted to a specific application.

Their extensive use in manufacturing components of MEMS [6], [2, Chapter 4] was driven by the requirement of better thermal properties than initially used raw materials - especially high thermal conductivity and low thermal expansion coefficient - along with adequate electric properties. Following this trend, several studies are being conducted for the past few years to extend the use of composites in manufacturing electromagnetic components of MEMS such as dielectric with electric high permittivity for capacitors [27] or magnetic core with high magnetic permeability for planar inductors [30]. It is also envisioned to use the flexibility in properties provided by composites to develop material with simultaneously high electric permittivity and high magnetic permeability to use a single material for both applications [18].

Within the families of composites, particle doped composites have been determined to be the most suitable for applications stated previously. These are made by embedding particles into an easily moldable base material that is usually designated as the matrix material. Particles with diameter ranging from nm to μm are sought for an overall composite material in the μm to mm range. A schematic of the microstructure of such a particle doped composite is shown in Figure 1.1.

These composites - like any other - have point wise variable properties: properties of the particles if we are inside a particle, otherwise properties of the matrix material. This description doesn't give proper quantitative information about the overall characteristics of the composite. Average properties obtained by homogenization, called effective properties [28], have been introduced for better characterization of the macroscopic response. For

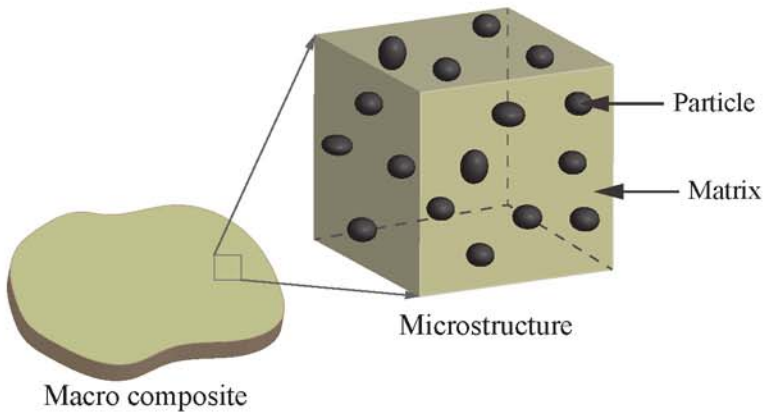

Figure 1.1: Schematic of the microstructure of a particle doped composite.

the electromagnetic device applications mentioned previously, estimating the effective electromagnetic properties of the composite, namely the effective electric permittivity and the effective magnetic permeability, is of prime importance in predicting its behavior and assessing the success of the newly designed composite.

Analytical bounds to the value of these effective electromagnetic properties exist. They could be evaluated knowing the constitution of the composite. Initial bounds were derived by Wiener in 1910 [29]. They allowed estimating a range for the effective electromagnetic properties of any kind of composite knowing the parent materials' properties and quantities. Then, in 1962 Hashin and Shtrikman [9] derived tighter bounds in the specific case of a composite made of two linear isotropic materials. The use of these bounds is however limited: they provide large range and don't take the microstructure of the composites into account. Numerical methods to estimate effective properties were first developed for effective mechanical properties - a detailed explanation can be found in [33]. Then, it was later extended to the numerical estimation of effective electromagnetic properties of spherical particle composites by Zohdi [34].

In the present study, we develop a numerical framework to estimate the effective electromagnetic properties for isotropic particulate composites in order to provide an accurate tool during their design for electromagnetic applications. Following [33, 34], it consists of building a numerical sample of the composite material of interest, and applying electromagnetic (EM) field at its interface. Then, Maxwell's equations [15] are solved numerically over the sample to obtain its electromagnetic response. Subsequently, the computed fields are averaged over the sample to estimate the effective properties using their definitions given in expressions 3.4 and 3.8. This method is designed to handle composites consisting of any number of isotropic phases and any particles shapes. The novelty also resides in the use of a Finite Difference Time Domain (FDTD) method specifically designed for Maxwell's equations, known as Yee's scheme [31]. Moreover, parallel implementation of the numerical

solver is done for high performance in computation. The method is then used to assess the thermal dependence of effective electromagnetic properties. A numerical design tool, that allows determining the required mixture parameters for a composite to achieve desired effective electromagnetic properties, is also developed. Throughout the study, stress, strain, and chemical effects are neglected, although the consideration of dynamic Maxwell's equations provide the possibility to consider these dynamic phenomena if required. Constituents and resulting composites are assumed to be linear, isotropic and non-dispersive.

The organization of this dissertation is as follows. In Chapter 2 a review of the electromagnetic theory, essential for this study, is presented. The homogenization process is discussed in chapter 3, where effective electromagnetic properties are introduced along with the existing analytical estimations of their values. In Chapter 4, a numerical method to compute the effective electromagnetic properties of a particle doped composites with known composition is presented. The method is extended in Chapter 5 to account for thermal effects. A numerical design tool that determines the required mixture parameters for a composite in achieving the desired effective electromagnetic properties, is developed in chapter 6. Finally, the dissertation ends with closing comments on the overall work presented and possible extensions to improve the method.

Chapter 2

Review of electromagnetic theory

Electric field, magnetic field and their governing equations are of key importance in this study. This chapter presents a review of electromagnetic theory. A detailed explanation on the subject could be found in [13], [7], and [14].

2.1 Introduction to electric field

The electric field could be seen as a physical field present in the neighborhood of any charged particle or time varying magnetic field. It is quantified by the electric field intensity **E**. For convenience, the electric flux density **D** is often introduced.

2.1.1 Electric field intensity E

A charge q (steady or moving) in an electric field would be subjected to a force given by Coulomb's law

$$\mathbf{F}_E = q\mathbf{E} \tag{2.1}$$

where **E** is the electric field intensity, expressed in Newton per Coulomb (N/C) or equivalently in V/m. The relation between electric field intensity, charge repartition and time varying magnetic field is expressed by Faraday's law and Gauss' law, presented in section 2.3.

2.1.2 Electric field density D

In dielectric materials all charges are attached to a specific atom. When an electric field is applied to it, the positive charges (nucleus) are pushed in the direction of the field and the negative charges (electron) are pushed in the opposite direction. Equilibrium is rapidly established between the field pushing the charges apart and their mutual attraction. The atom is then polarized with positive charges on one side and negative charges on the other.

We say that dielectrics polarize in response to an applied electric field. It is shown that the effect of polarization is to produce charge density ρ_b called bound charge within the dielectric, and surface charge λ_b called bound surface charge on its surface. At a macroscopic level, a polarization field $\mathbf{P}$ that tends to oppose the applied field $\mathbf{E}$ is generated. This field is simply the field due to the bound charges, such that

$$\rho_b = -\nabla \cdot \mathbf{P} \tag{2.2}$$
$$\lambda_b = \mathbf{P} \cdot \mathbf{n} \tag{2.3}$$

where $\mathbf{n}$ is the unit normal vector at the surface of the matter.

It is convenient to introduce a new quantity called electric field displacement or electric flux density, denoted $\mathbf{D}$ and expressed in C/m^2, such that

$$\mathbf{D} = \epsilon_0 \mathbf{E} + \mathbf{P} \tag{2.4}$$

where $\epsilon_0 = \frac{1}{4\pi 10^{-7} c^2}$ is the permittivity constant of free space expressed in F/m, with c being the speed of light in free space. As we will see later, it allows expressing Maxwell's equations in term of the free charges only, which are known quantities.

2.2 Introduction to magnetic field

The magnetic field could be seen as a physical field present in the neighborhood of any currents (moving charges) or time varying electric field. It is quantified by the magnetic flux density $\mathbf{B}$. For convenience, the magnetic field intensity $\mathbf{H}$ is often introduced.

2.2.1 Magnetic field density B

A charge q moving at velocity $\mathbf{v}$ and passing in a region where a magnetic field is present would experience a force called Lorentz. It is given by

$$\mathbf{F}_B = q(\mathbf{v} \times \mathbf{B}) \tag{2.5}$$

where $\mathbf{B}$ is the magnetic flux density, expressed in Tesla (T). The relation between magnetic flux density, current repartition and time varying electric field is expressed by Ampere's law and Gauss' law for magnetism, presented in section 2.3.

2.2.2 Magnetic field intensity H

Inside an atom, electrons are orbiting with randomly oriented orbits, canceling out the orbital dipole moment of the atom. In presence of a magnetic field, each electron experiences

an extra force: Lorentz force. They thus pick up an extra dipole moment. We say that the matter becomes magnetized, that is each atom acquires a dipole moment. It is described at the macroscopic level by the magnetization field $\mathbf{M}$. It is shown that the effect of magnetization is to produce current density $\mathbf{J}_b$ called bound current within the matter, and surface current $\mathbf{j}_b$, called bound surface current, on its surface. The magnetization field is then simply the field due to this currents, such that

$$\mathbf{J}_b = \nabla \times \mathbf{M} \tag{2.6}$$
$$\mathbf{j}_b = \mathbf{M} \times \mathbf{n} \tag{2.7}$$

where $\mathbf{n}$ is the unit normal vector at the surface of the matter.

It is convenient to introduce a new quantity called magnetic field intensity, denoted $\mathbf{H}$ and expressed in A/m, such that

$$\mathbf{H} = \frac{\mathbf{B}}{\mu_0} - \mathbf{M} \tag{2.8}$$

where $\mu_0 = 4\pi 10^{-7}$ is the magnetic permeability constant of free space expressed in H/m. As we will see later, it allows expressing Maxwell's equations in term of the free currents only, which are known quantities.

2.3 Maxwell's equations

Maxwell's equations are concise way to state the fundamentals of electromagnetism. They are a set of four coupled partial differential equations derived empirically, relating the electromagnetic fields characteristic quantities ($\mathbf{E}$, $\mathbf{D}$, $\mathbf{B}$, $\mathbf{H}$) to the charge distribution and current distribution in a system. They are presented next in their upmost general form: the integral form.

For the next sections, we choose our domain of interest to be a randomly shaped material of volume Ω. Then, $\mathcal{C}$ is a randomly chosen closed curve in Ω, Γ is a surface generated by $\mathcal{C}$, $\mathcal{S}$ is a randomly chosen closed surface in Ω, and $\mathcal{V}$ is the volume generated by $\mathcal{S}$.

2.3.1 Faraday's law

Faraday's law expresses that a changing magnetic field induces an electric field:

$$\oint_{\mathcal{C}} \mathbf{E} \cdot d\mathbf{l} = -\iint_{\Gamma} \frac{\partial \mathbf{B}}{\partial t} \cdot d\mathbf{\Gamma} \tag{2.9}$$

where $d\mathbf{l} = dl\mathbf{t}$ with dl being an infinitesimal element of $\mathcal{C}$ oriented by the unit tangential vector $\mathbf{t}$, and $d\mathbf{\Gamma} = d\Gamma\mathbf{n}$ with $d\Gamma$ being an infinitesimal element of Γ oriented by the outer unit normal vector $\mathbf{n}$. This is illustrated in Figure 2.1.

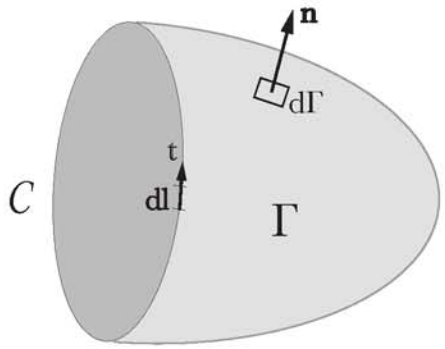

Figure 2.1: Illustration of the notations used for closed curve integrals.

2.3.2 Ampere's law

Ampere's law - with Maxwell's fix - states that electric currents and changing electric field induce a magnetic field:

$$\oint_{\mathcal{C}} \mathbf{H} \cdot d\mathbf{l} = \iint_{\Gamma} \left(\mathbf{J}_f + \frac{\partial \mathbf{D}}{\partial t} \right) \cdot d\mathbf{\Gamma} \tag{2.10}$$

where $\mathbf{J}_f$, expressed in A/m^2, represents the free currents in the matter.

2.3.3 Gauss' law

Gauss' law states that the total electric flux through any closed surface $\mathcal{S}$ is equal to the free electric charge enclosed within $\mathcal{S}$:

$$\oiint_{\mathcal{S}} \mathbf{D} \cdot d\mathbf{S} = Q_f \tag{2.11}$$

where Q_f (in C) represent the free charges included in the volume $\mathcal{V}$ generated by $\mathcal{S}$, and $d\mathbf{S} = dS\mathbf{n}$ with dS being an infinitesimal element of $\mathcal{S}$ oriented by the outer unit normal vector $\mathbf{n}$. This is illustrated in Figure 2.2.

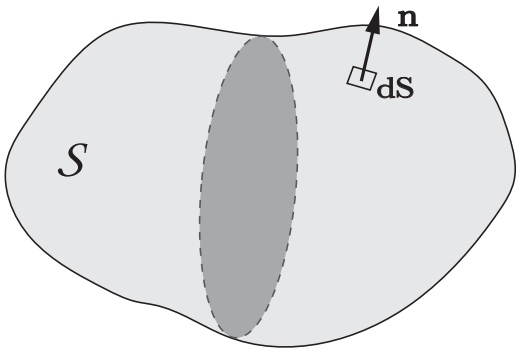

Figure 2.2: Illustration of the notations used for closed surface integral.

2.3.4 Gauss' law for magnetism

The following law has actually no name, but is often referred to as Gauss' law for magnetism. It states that the total magnetic flux through any closed surface $\mathcal{S}$ is always zero:

$$\oiint_{\mathcal{S}} \mathbf{B} \cdot d\mathbf{A} = 0 \tag{2.12}$$

2.4 Local form of Maxwell's equations

It is possible to localize the previous integral equations to obtain the so-called local form of Maxwell's equations. They are much more convenient, especially for numerical analysis, as they give a pointwise relation between the different electromagnetic quantities. They are derived next. We will see that each integral equation gives two local equations that hold alternatively: differential form when the fields are smooth enough, and jump or discontinuity conditions when discontinuities in the fields occur.

2.4.1 Local Faraday's law

Let's assume first that $\mathbf{E}$ is spatially differentiable over the surface Γ. We can then apply Stokes' theorem to the left integral of equation 2.9:

$$\oint_{\mathcal{C}} \mathbf{E} \cdot d\mathbf{l} = \iint_{\Gamma} (\nabla \times \mathbf{E}) \cdot d\mathbf{\Gamma} \tag{2.13}$$

Plugging back into the original equation we get

$$\int_{\Gamma} (\nabla \times \mathbf{E}) \cdot d\mathbf{\Gamma} = -\int_{\Gamma} \frac{\partial \mathbf{B}}{\partial t} \cdot d\mathbf{\Gamma} \tag{2.14}$$

Let's assume that $\nabla \times \mathbf{E}$ and $\frac{\partial \mathbf{B}}{\partial t}$ are spatially continuous over Γ. As Γ is randomly chosen, we can apply localization theorem to obtain the local relation at any point in space where the previous differentiability and continuity assumptions hold:

$$\frac{\partial \mathbf{B}}{\partial t} = -\nabla \times \mathbf{E} \tag{2.15}$$

This is derived assuming that the concerned fields are smooth enough, starting from the electric field intensity $\mathbf{E}$. Now assume that there exist a surface Σ in Ω where $\mathbf{E}$ is not spatially differentiable (we don't discuss the cause for this yet, this will be done later). Then, we cannot apply Stokes' theorem at Σ as $\nabla \times \mathbf{E}$ is not defined there. To derive the local relation at a point of Σ we proceed as following. We take a curve $\mathcal{C}$ around the surface of discontinuity Σ with Γ being the surface generated by our curve. Then, we divide the curve into two parts on both side of the surface Σ such that $\mathcal{C} = \mathcal{C}^- \cup \mathcal{C}^+$ and $\Gamma = \Gamma^- \cup \Gamma^+$, as shown in figure 2.3. We call γ the intersection between Σ and Γ. Let's apply Faraday's law over each of these curves individually:

$$\begin{aligned} &\oint_{\mathcal{C}^- \cup \gamma} \mathbf{E} \cdot d\mathbf{l} = -\iint_{\Gamma^-} \frac{\partial \mathbf{B}}{\partial t} \cdot d\mathbf{\Gamma} \\ \rightarrow &\int_{\mathcal{C}^-} \mathbf{E} \cdot d\mathbf{l} + \int_{\gamma} \mathbf{E}^- \cdot \mathbf{t}_\gamma dl = -\iint_{\Gamma^-} \frac{\partial \mathbf{B}}{\partial t} \cdot d\mathbf{\Gamma} \end{aligned} \tag{2.16}$$

$$\begin{aligned} &\oint_{\mathcal{C}^+ \cup \gamma} \mathbf{E} \cdot d\mathbf{l} = -\iint_{\Gamma^+} \frac{\partial \mathbf{B}}{\partial t} \cdot d\mathbf{\Gamma} \\ \rightarrow &\int_{\mathcal{C}^+} \mathbf{E} \cdot d\mathbf{l} + \int_{\gamma} \mathbf{E}^+ \cdot (-\mathbf{t}_\gamma)\, dl = -\iint_{\Gamma^+} \frac{\partial \mathbf{B}}{\partial t} \cdot d\mathbf{\Gamma} \end{aligned} \tag{2.17}$$

Summing both gives

$$\oint_{\mathcal{C}} \mathbf{E} \cdot d\mathbf{l} - \int_{\gamma} \left(\mathbf{E}^+ - \mathbf{E}^-\right) \cdot \mathbf{t}_\gamma dl = -\iint_{\Gamma} \frac{\partial \mathbf{B}}{\partial t} \cdot d\mathbf{\Gamma} \tag{2.18}$$

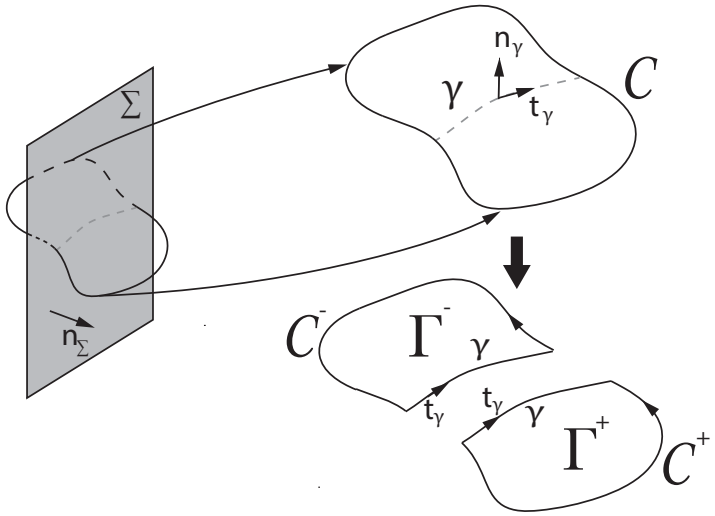

Figure 2.3: Illustration of a curve $\mathcal{C}$ around a surface of discontinuity Σ.

From applying Faraday's law to $\mathcal{C}$ we have

$$\oint_{\mathcal{C}} \mathbf{E} \cdot d\mathbf{l} = -\iint_{\Gamma} \frac{\partial \mathbf{B}}{\partial t} \cdot d\mathbf{\Gamma} \tag{2.19}$$

After subtracting 2.19 from 2.18 we are left with

$$\int_{\gamma} \left(\mathbf{E}^{+} - \mathbf{E}^{-}\right) \cdot \mathbf{t}_{\gamma} dl = 0 \tag{2.20}$$

Since $\mathcal{C}$ is randomly chosen, so is γ. Hence, we can conclude by localization that at any point of a surface of discontinuity we have

$$\left(\mathbf{E}^{+} - \mathbf{E}^{-}\right) \cdot \mathbf{t}_{\gamma} = 0 \tag{2.21}$$

We can always choose Γ such that $\mathbf{t}_{\gamma} = \mathbf{n}_{\gamma} \times \mathbf{n}_{\Sigma}$ where $\mathbf{n}_{\gamma}$ is the unit normal to Γ at the curve γ and $\mathbf{n}_{\Sigma}$ is the unit normal to Σ at the curve γ pointing from the $-$ side to the $+$ side. We then have

$$\left(\mathbf{E}^{+} - \mathbf{E}^{-}\right) \cdot \left(\mathbf{n}_{\gamma} \times \mathbf{n}_{\Sigma}\right) = 0 \tag{2.22}$$

$$\rightarrow \quad \mathbf{n}_{\gamma} \cdot \left(\mathbf{n}_{\Sigma} \times \left(\mathbf{E}^{+} - \mathbf{E}^{-}\right)\right) = 0 \tag{2.23}$$

Finally

$$\mathbf{n}_\Sigma \times \left(\mathbf{E}^+ - \mathbf{E}^-\right) = 0 \tag{2.24}$$

This tells us that even at a surface where $\mathbf{E}$ would be discontinuous, the components of $\mathbf{E}$ tangential to this surface are always continuous. Hence, a potential discontinuity in $\mathbf{E}$ would only come from its component normal to the surface of discontinuity.

2.4.2 Local Ampere's law

The local forms of Ampere's law are derived similarly. Let's assume first that $\mathbf{H}$ is spatially differentiable over the surface Γ. We can then apply Stokes' theorem to the left integral of equation 2.10:

$$\oint_{\mathcal{C}} \mathbf{H} \cdot d\mathbf{l} = \int_{\Gamma} (\nabla \times \mathbf{H}) \cdot d\mathbf{\Gamma} \tag{2.25}$$

Plugging back into the original equations we get

$$\int_{\Gamma} (\nabla \times \mathbf{H}) \cdot d\mathbf{\Gamma} = \iint_{\Gamma} \left(\mathbf{J}_f + \frac{\partial \mathbf{D}}{\partial t}\right) \cdot d\mathbf{\Gamma} \tag{2.26}$$

Let's assume that $\nabla \times \mathbf{H}$ and $\frac{\partial \mathbf{D}}{\partial t}$ are spatially continuous over Γ. As Γ is randomly chosen, we can apply localization theorem to obtain the local relation at any point in space where the previous differentiability and continuity assumptions hold:

$$\frac{\partial \mathbf{D}}{\partial t} + \mathbf{J}_f = \nabla \times \mathbf{H} \tag{2.27}$$

To derive the local relation at a point of a surface of discontinuity we proceed exactly as for Faraday's law. An extra assumption is made: we assume that a free surface current $\mathbf{j}_f$ is going through the assumed surface of discontinuity Σ. Let's apply now Ampere's law over each of the two curves individually:

$$\begin{aligned} \oint_{\mathcal{C}^- \cup \gamma} \mathbf{H} \cdot d\mathbf{l} &= \iint_{\Gamma^-} \left(\mathbf{J}_f + \frac{\partial \mathbf{D}}{\partial t}\right) \cdot d\mathbf{\Gamma} \\ \rightarrow \int_{\mathcal{C}^-} \mathbf{H} \cdot d\mathbf{l} + \int_{\gamma} \mathbf{H}^- \cdot \mathbf{t}_\gamma dl &= \iint_{\Gamma^-} \left(\mathbf{J}_f + \frac{\partial \mathbf{D}}{\partial t}\right) \cdot d\mathbf{\Gamma} \end{aligned} \tag{2.28}$$

$$\oint_{\mathcal{C}^+\cup\,\gamma} \mathbf{H}\cdot d\mathbf{l} = \iint_{\Gamma^+} \left(\mathbf{J}_f + \frac{\partial \mathbf{D}}{\partial t}\right)\cdot d\mathbf{\Gamma}$$

$$\rightarrow \int_{\mathcal{C}^+} \mathbf{H}\cdot d\mathbf{l} + \int_{\gamma} \mathbf{H}^+\cdot(-\mathbf{t}_\gamma)\, dl = \iint_{\Gamma^+} \left(\mathbf{J}_f + \frac{\partial \mathbf{D}}{\partial t}\right)\cdot d\mathbf{\Gamma} \tag{2.29}$$

Summing both gives

$$\int_{\mathcal{C}} \mathbf{H}\cdot d\mathbf{l} - \int_{\gamma} \left(\mathbf{H}^+ - \mathbf{H}^-\right)\cdot \mathbf{t}_\gamma dl = \iint_{\Gamma} \left(\mathbf{J}_f + \frac{\partial \mathbf{D}}{\partial t}\right)\cdot d\mathbf{\Gamma} \tag{2.30}$$

From applying Ampere's law to $\mathcal{C}$ we have

$$\oint_{\mathcal{C}} \mathbf{H}\cdot d\mathbf{l} = \iint_{\Gamma} \left(\mathbf{J}_f + \frac{\partial \mathbf{D}}{\partial t}\right)\cdot d\mathbf{\Gamma} + \int_{\gamma} \mathbf{j}_f\cdot \mathbf{n}_\gamma dl \tag{2.31}$$

By subtracting 2.31 from 2.30 we get

$$\int_{\gamma} \left(\mathbf{H}^+ - \mathbf{H}^-\right)\cdot \mathbf{t}_\gamma dl = \int_{\gamma} \mathbf{j}_f\cdot \mathbf{n}_\gamma dl \tag{2.32}$$

As $\mathcal{C}$ is randomly chosen, so is γ. Hence, we can conclude by localization that at any point of a surface of discontinuity we have

$$\left(\mathbf{H}^+ - \mathbf{H}^-\right)\cdot \mathbf{t}_\gamma = \mathbf{j}_f\cdot \mathbf{n}_\gamma \tag{2.33}$$

By proceeding as previously we get

$$\mathbf{n}_\Sigma \times \left(\mathbf{H}^+ - \mathbf{H}^-\right) = \mathbf{j}_f \tag{2.34}$$

This tells us that the components of $\mathbf{H}$ tangential to a surface where a free surface current is present are discontinuous. Across a surface where no such current is present the components of $\mathbf{H}$ tangential to this surface are always continuous.

2.4.3 Local Gauss' law

Assuming a volume distribution ρ_f of free charge over the volume $\mathcal{V}$, Gauss' law integral form 2.11 can be written as

$$\oiint_{\mathcal{S}} \mathbf{D} \cdot d\mathbf{S} = \iiint_{\mathcal{V}} \rho_f dV \tag{2.35}$$

Let's assume that $\mathbf{D}$ is spatially differentiable over the volume $\mathcal{V}$. We can then apply divergence theorem to the left integral of equation 2.35:

$$\oiint_{\mathcal{S}} \mathbf{D} \cdot d\mathbf{S} = \iiint_{\mathcal{V}} \nabla \cdot \mathbf{D} \; dV \tag{2.36}$$

Plugging back into the original equations we get

$$\iiint_{\mathcal{V}} \nabla \cdot \mathbf{D} \; d\mathbf{V} = \iiint_{\mathcal{V}} \rho_f dV \tag{2.37}$$

Let's assume that $\nabla \cdot \mathbf{D}$ and ρ_f are continuous over $\mathcal{V}$. As $\mathcal{V}$ is randomly chosen, we can apply localization theorem to obtain the local relation at any point in space where the previous differentiability and continuity assumptions hold:

$$\nabla \cdot \mathbf{D} = \rho_f \tag{2.38}$$

This is derived assuming that the concerned fields are smooth enough, starting from the electric field density $\mathbf{D}$. Now assume - as previously - that there exist a surface Σ in Ω where $\mathbf{D}$ is not smooth i.e. where it is not differentiable. Then, we cannot apply the divergence theorem at Σ as $\nabla \cdot \mathbf{D}$ is not defined there.

To derive the local relation at a point of the surface of discontinuity we proceed as following. Let's assume there exist a free surface charge distribution λ_f over Σ. Let's take a surface $\mathcal{S}$ around the surface of discontinuity Σ. Then, let's divide the surface into two parts on both side of Σ such that $\mathcal{S} = \mathcal{S}^- \cup \mathcal{S}^+$ and $\mathcal{V} = \mathcal{V}^- \cup \mathcal{V}^+$, as shown in figure 2.4. We can apply Gauss' law over each of these surfaces individually

$$\begin{aligned} &\oiint_{\mathcal{S}^- \cup \, a} \mathbf{D} \cdot d\mathbf{S} = \iiint_{\mathcal{V}^-} \rho_f dV \\ \rightarrow \quad &\iint_{\mathcal{S}^-} \mathbf{D} \cdot d\mathbf{S} + \iint_{a} \mathbf{D}^- \cdot \mathbf{n}_\Sigma dS = \iiint_{\mathcal{V}^-} \rho_f dV \end{aligned} \tag{2.39}$$

$$\oiint_{\mathcal{S}^+\cup\, a} \mathbf{D}\cdot d\mathbf{S} = \iiint_{\mathcal{V}^+} \rho_f dV$$
$$\rightarrow \iint_{\mathcal{S}^+} \mathbf{D}\cdot d\mathbf{S} + \iint_{a} \mathbf{D}^+\cdot(-\mathbf{n}_\Sigma)dS = \iiint_{\mathcal{V}^+} \rho_f dV \tag{2.40}$$

Summing both gives

$$\iint_{\mathcal{S}} \mathbf{D}\cdot d\mathbf{S} - \iint_{a} \left(\mathbf{D}^+ - \mathbf{D}^-\right)\cdot \mathbf{n}_\Sigma dS = \iiint_{\mathcal{V}} \rho_f dV \tag{2.41}$$

From applying Gauss' law to $\mathcal{S}$ we have

$$\oiint_{\mathcal{S}} \mathbf{D}\cdot d\mathbf{S} = \iiint_{\mathcal{V}} \rho_f dV + \iint_{a} \lambda_f dS \tag{2.42}$$

By subtracting equation 2.42 from 2.41 we get

$$\iint_{a} \left(\mathbf{D}^+ - \mathbf{D}^-\right)\cdot \mathbf{n}_\Sigma dS = \iint_{a} \lambda_f dS \tag{2.43}$$

As $\mathcal{S}$ is chosen randomly, so is a. Thus, we have by localization

$$\left(\mathbf{D}^+ - \mathbf{D}^-\right)\cdot \mathbf{n}_\Sigma = \lambda_f \tag{2.44}$$

This tells us that the component of $\mathbf{D}$ normal to a surface where a free surface charge distribution is present is discontinuous. Across a surface where no such charge distribution is present the component of $\mathbf{D}$ normal to this surface is always continuous.

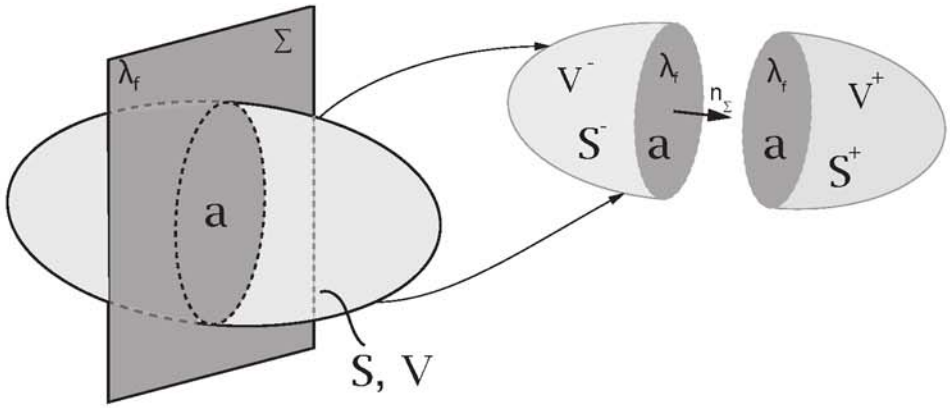

Figure 2.4: Illustration of a volume $\mathcal{V}$ around a surface of discontinuity Σ.

2.4.4 Local Gauss' law for magnetism

We proceed as previously to obtain the differential form of equation 2.12. In the case $\mathbf{B}$ is smooth we have locally

$$\nabla \cdot \mathbf{B} = 0 \tag{2.45}$$

Similarly as for Gauss' law we obtain at a point on a surface of potential discontinuity

$$(\mathbf{B}^+ - \mathbf{B}^-) \cdot \mathbf{n}_\Sigma = 0 \tag{2.46}$$

This tells us that the component of $\mathbf{B}$ normal to any surface is always continuous. Any potential discontinuity in $\mathbf{B}$ at a surface is due to its components tangential to such surface.

2.5 Hidden charge conservation law

A fundamental assumption in electromagnetism is that electric charges are conserved. In other word if the total charge in a region has changed, it is because charge has passed out of the region or entered into it through the bounding surface. This is expressed mathematically by the charge conservation law

$$\frac{\partial Q_f}{\partial t} = - \oiint_{\mathcal{S}} \mathbf{J}_f \cdot d\mathbf{S} \tag{2.47}$$

where Q_f (in C) represent the total free charges included in the volume $\mathcal{V}$ generated by $\mathcal{S}$.

It turns out that the charge conservation law is included into Maxwell's equations. To show this, let's take the time derivative of the Gauss' law in integral form 2.11

$$\frac{\partial}{\partial t} \oiint_{\mathcal{S}} \mathbf{D} \cdot d\mathbf{S} = \frac{\partial Q_f}{\partial t} \tag{2.48}$$

As no deformation are considered we can move the time derivative inside the integral

$$\oiint_{\mathcal{S}} \frac{\partial \mathbf{D}}{\partial t} \cdot d\mathbf{S} = \frac{\partial Q_f}{\partial t} \tag{2.49}$$

Using Ampere's law in integral form 2.10, we have

$$\oint_{\mathcal{C}_\mathcal{S}} \mathbf{H} \cdot d\mathbf{l} - \oiint_{\mathcal{S}} \mathbf{J}_f \cdot d\mathbf{S} = \frac{\partial Q_f}{\partial t} \tag{2.50}$$

where $\mathcal{C}_\mathcal{S}$ is the closed curve generating $\mathcal{S}$. As $\mathcal{S}$ is a closed surface, this curve is the zero curve. Hence, we obtain the charge conservation law

$$\frac{\partial Q_f}{\partial t} = -\oiint_{\mathcal{S}} \mathbf{J}_f \cdot d\mathbf{S} \tag{2.51}$$

Thus, for any electromagnetism problem it is sufficient to solve only Maxwell's equations as the charge conservation is incorporated in them.

2.6 Remark on interconnection between the Maxwell's equations

Let's first take the divergence of the differential Faraday's law

$$\nabla \cdot \left(\frac{\partial \mathbf{B}}{\partial t} \right) = -\nabla \cdot (\nabla \times \mathbf{E}) = 0 \tag{2.52}$$

$$\rightarrow \frac{\partial}{\partial t} (\nabla \cdot \mathbf{B}) = 0 \tag{2.53}$$

Hence, Gauss' law for magnetism is time independent: if satisfied initially it is always satisfied.

Similarly let's take the divergence of the differential Ampere's law

$$\nabla \cdot \left(\frac{\partial \mathbf{D}}{\partial t} \right) = \nabla \cdot (\nabla \times \mathbf{H} - \mathbf{J}_f) = -\nabla \cdot \mathbf{J}_f \tag{2.54}$$

$$\rightarrow \frac{\partial}{\partial t} (\nabla \cdot \mathbf{D}) = -\nabla \cdot \mathbf{J}_f \tag{2.55}$$

From the charge conservation law

$$\frac{\partial}{\partial t} (\nabla \cdot \mathbf{D}) = \frac{\partial \rho_f}{\partial t} \tag{2.56}$$

$$\rightarrow \frac{\partial}{\partial t} (\nabla \cdot \mathbf{D} - \rho_f) = 0 \tag{2.57}$$

Hence, Gauss' law is time independent: if satisfied initially it is always satisfied.

This shows that when solving Maxwell's equations numerically - as we will do in chapter 4 - it is enough to solve only the time dependent equations if the divergence equations are satisfied as initial conditions. Of course, all the interface conditions must be implemented properly when required.

2.7 Linear isotropic materials

2.7.1 Electric permittivity

For many materials, commonly designated as linear isotropic, the polarization $\mathbf{P}$ is proportional to the electric field intensity $\mathbf{E}$, such that

$$\mathbf{P} = \epsilon_0 \chi_e \mathbf{E} \tag{2.58}$$

The constant χ_e is called the electric susceptibility of the material (dimensionless). It indicates the degree of polarization of a material in response to an applied electric field.

The electric displacement for such material is expressed as

$$\mathbf{D} = \epsilon_0 \mathbf{E} + \mathbf{P} = \epsilon_0 (1 + \chi_e) \mathbf{E} \tag{2.59}$$

Hence, $\mathbf{D}$ is also proportional to $\mathbf{E}$. We introduce the constant of proportionality ϵ, expressed in F/m such that

$$\epsilon = \epsilon_0(1 + \chi_e) \tag{2.60}$$

It is called the electric permittivity of the material. Note that it does carry the same information as χ_e: it measures the resistance that is encountered when forming an electric field inside a material. Either one of them is given for a material. Most often, the relative electric permittivity is listed

$$\epsilon_r = \frac{\epsilon}{\epsilon_0} = 1 + \chi_e \tag{2.61}$$

2.7.2 Magnetic permeability

Similarly, for most materials, designated again as linear isotropic, the magnetization $\mathbf{M}$ is proportional to the magnetic field density $\mathbf{H}$ such that

$$\mathbf{M} = \chi_m \mathbf{H} \tag{2.62}$$

The constant χ_m is called the magnetic susceptibility of the material (dimensionless). It indicates the degree of magnetization of a material in response to an applied magnetic field.

The magnetic displacement for such material is expressed as

$$\mathbf{B} = \mu_0 (\mathbf{H} + \mathbf{M}) = \mu_0(1 + \chi_m)\mathbf{H} \tag{2.63}$$

Hence, $\mathbf{B}$ is also proportional to $\mathbf{H}$. We introduce the constant of proportionality μ, expressed in H/m such that

$$\mu = \mu_0(1 + \chi_m) \tag{2.64}$$

It is called the magnetic permeability of the material. Note that it does carry the same information as χ_m: it measures the ability of a material to support the formation of a magnetic field within itself. Either one of them is given for a material. Most often, the relative magnetic permeability is listed

$$\mu_r = \frac{\mu}{\mu_0} = 1 + \chi_m \tag{2.65}$$

2.7.3 Electric conductivity

We assume is this study that the only free currents we have are conductive currents. Assuming Ohm's law hold, we have for linear isotropic materials

$$\mathbf{J}_c = \sigma \mathbf{E} \tag{2.66}$$

where σ is the electric conductivity, expressed in S/m.

2.8 Summary

We will work next assuming that the material we are working with are linear isotropic. Moreover, no free surface charges or free surface currents would be considered. Under those assumptions we can express Maxwell's equations only in terms of $\mathbf{E}$ and $\mathbf{H}$. We have in case of smooth fields

$$\frac{\partial (\mu \mathbf{H})}{\partial t} = -\nabla \times \mathbf{E} \tag{2.67}$$

$$\frac{\partial (\epsilon \mathbf{E})}{\partial t} + \sigma \mathbf{E} = \nabla \times \mathbf{H} \tag{2.68}$$

$$\nabla \cdot (\epsilon \mathbf{E}) = 0 \tag{2.69}$$

$$\nabla \cdot (\mu \mathbf{H}) = 0 \tag{2.70}$$

At point of a surface with potential discontinuities we have

$$\mathbf{n} \times \left(\mathbf{E}^+ - \mathbf{E}^-\right) = \mathbf{0} \tag{2.71}$$

$$\mathbf{n} \times \left(\mathbf{H}^+ - \mathbf{H}^-\right) = \mathbf{0} \tag{2.72}$$

$$\left((\epsilon \mathbf{E})^+ - (\epsilon \mathbf{E})^-\right) \cdot \mathbf{n} = 0 \tag{2.73}$$

$$\left((\mu \mathbf{H})^+ - (\mu \mathbf{H})^-\right) \cdot \mathbf{n} = 0 \tag{2.74}$$

where $\mathbf{n}$ is the normal at the surface of discontinuity.

We can now clearly identify these potential causes of discontinuity in this particular case. We can see from 2.71 that the tangential components of $\mathbf{E}$ at any surface are always continuous. However, we see from 2.73 that the component of $\mathbf{E}$ normal to an interface between two materials with different electric permittivity ϵ would be discontinuous. Hence, equations 2.67 and 2.69 involving spatial derivatives of $\mathbf{E}$ don't apply at such location, we should rather

use the corresponding interface conditions 2.71 and 2.73.

Similarly we see from 2.72 that the tangential components of **H** at any surface are always continuous. However, we see from 2.74 that the component of **H** normal to an interface between two materials with different magnetic permeability μ would be discontinuous. Hence, equations 2.68 and 2.70 involving spatial derivatives of **H** don't apply at such location, we should rather use the corresponding interface conditions 2.72 and 2.74.

Chapter 3

Effective electromagnetic properties

Homogenization and effective properties are of key importance in this study. Homogenization process is presented first in this chapter. Then, the two effective properties of interest are defined: the effective electric permittivity and the effective magnetic permeability. Analytical bounds available to their values are introduced. Finally, their limitations and the requirements for better estimation are discussed.

3.1 Homogenization and effective properties

If we look at sufficiently fine scale all materials are heterogeneous, made of individual atoms, which are themselves made of electrons, neutrons and protons. To characterize a material exactly, the effect of each of these individual entities and their interaction should be taken into account. Given their uncountable number, this would be an impossible task. To overcome this difficulty, the hypothesis of continuous material has been introduced. This hypothesis proposes a notion of average properties in which the actual constitution of the material is idealized by considering the material to be continuous. A homogeneous medium is then characterized by properties that are identical at every point.

The same homogenization process is used to characterize particle doped materials. The properties of a composite are point wise variable. For instance, if we are looking at a property P, the composite will have the property P_p of particles at location where particles are present and property P_m of matrix material otherwise. However this does not give a proper quantification of the overall composite vis-à-vis the property P. To obtain a better characterization, we assume a homogenous form at macro level and define average properties that are identical at every point. This homogenization process is illustrated in Figure 3.1. The average properties are usually designated as effective properties and denoted using the superscript "*". We refer to [28] for a meticulous explanation of the topic.

In the next sections we discuss about the two effective properties of interest: the effective electric permittivity ϵ^*, and the effective magnetic permeability μ^*.

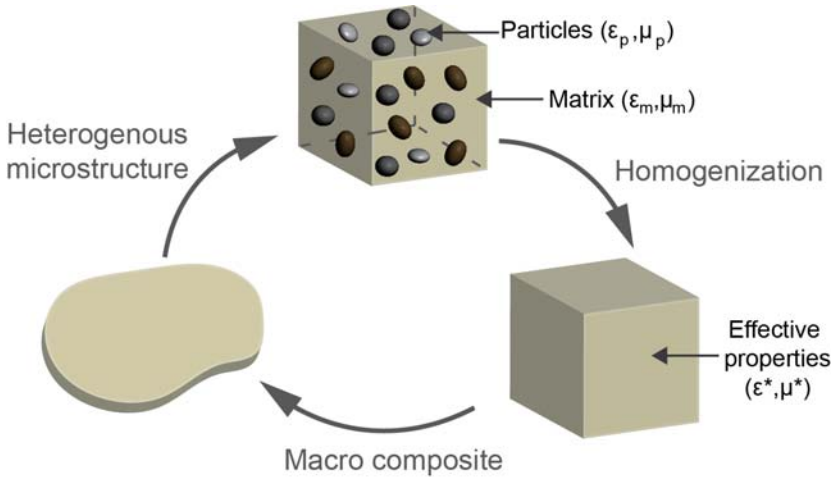

Figure 3.1: Homogenization of particle doped composites.

3.2 Effective electric permittivity

For a linear isotropic composite the effective permittivity, denoted as ϵ^*, is defined as following

$$\langle \mathbf{D} \rangle_\Omega = \epsilon^* \langle \mathbf{E} \rangle_\Omega \tag{3.1}$$

where Ω is the volume of the composite material, and $\langle \mathbf{D} \rangle_\Omega$ and $\langle \mathbf{E} \rangle_\Omega$ are respectively the average electric flux density and average electric field intensity over the volume Ω. The averaging operator $\langle . \rangle_\Omega$ applies to each component of $\mathbf{D}$ and $\mathbf{E}$. It is defined for any function f as

$$\langle f \rangle_\Omega = \frac{1}{|\Omega|} \int_\Omega f \mathrm{d}\Omega \tag{3.2}$$

Taking the dot product of the left and right hand side in equation 3.1, leads to

$$\langle \mathbf{D} \rangle_\Omega . \langle \mathbf{D} \rangle_\Omega = (\epsilon^*)^2 (\langle \mathbf{E} \rangle_\Omega . \langle \mathbf{E} \rangle_\Omega) \tag{3.3}$$

We can then extract the effective electric permittivity as

$$\epsilon^* = \sqrt{\frac{\langle \mathbf{D} \rangle_\Omega . \langle \mathbf{D} \rangle_\Omega}{\langle \mathbf{E} \rangle_\Omega . \langle \mathbf{E} \rangle_\Omega}} \tag{3.4}$$

The relative effective electric permittivity is often used which is expressed as

$$\epsilon_r^* = \frac{\epsilon^*}{\epsilon_0} \tag{3.5}$$

3.3 Effective magnetic permeability

For a linear isotropic composite the effective magnetic permeability, denoted as μ^*, is defined as following

$$\langle \mathbf{B} \rangle_\Omega = \mu^* \langle \mathbf{H} \rangle_\Omega \tag{3.6}$$

where Ω is the volume of the composite material, and $\langle \mathbf{B} \rangle_\Omega$ and $\langle \mathbf{H} \rangle_\Omega$ are respectively the average magnetic flux density and average magnetic field intensity over the volume Ω.

Taking the dot product of the left and right hand side by themselves in equation 3.6, leads to

$$\langle \mathbf{B} \rangle_\Omega . \langle \mathbf{B} \rangle_\Omega = (\mu^*)^2 (\langle \mathbf{H} \rangle_\Omega . \langle \mathbf{H} \rangle_\Omega) \tag{3.7}$$

We can then extract the effective magnetic permeability as

$$\mu^* = \sqrt{\frac{\langle \mathbf{B} \rangle_\Omega . \langle \mathbf{B} \rangle_\Omega}{\langle \mathbf{H} \rangle_\Omega . \langle \mathbf{H} \rangle_\Omega}} \tag{3.8}$$

The relative effective magnetic permeability is often used, given by

$$\mu_r^* = \frac{\mu^*}{\mu_0} \tag{3.9}$$

3.4 Analytical estimations

Analytically evaluating the effective properties of a composite material is not an easy task, even when its constitution is known. Several attempts have been made to derive analytical approximation. The most widely used analytical bounds are introduced next.

The subscript m designates a property of the matrix material, whereas p designates a property of the particles.

3.4.1 Wiener bounds

The widest bounds are the so-called Wiener bounds [29], developed in 1910. It was shown that the weighted average of the individual properties of each constituent gives an upper bound and their harmonic average gives a lower bound to the value of the effective properties. General formulations were derived for bounds valid for any type of linear composites. Their formulation in the case of a composite made with two linear isotropic materials is given below.

For the effective electrical permittivity ϵ^* we have

$$\left(\frac{v_m}{\epsilon_m} + \frac{v_p}{\epsilon_p}\right)^{-1} \leq \epsilon^* \leq v_m\epsilon_m + v_p\epsilon_p \tag{3.10}$$

Similarly, for the effective magnetic permeability we have

$$\left(\frac{v_m}{\mu_m} + \frac{v_p}{\mu_p}\right)^{-1} \leq \mu^* \leq v_m\mu_m + v_p\mu_p \tag{3.11}$$

where v_m and v_p refers to the volume fractions of the matrix and particles respectively.

3.4.2 Hashin and Shtrikman bounds

Improved bounds, valid only in the case of linear isotropic materials, were developed in 1962 by Hashin and Shtrikman [9]. Their formulations are as follow

$$\epsilon_1 + \frac{v_2^\epsilon}{\frac{1}{\epsilon_2-\epsilon_1} + \frac{1-v_2^\epsilon}{3\epsilon_1}} \leq \epsilon^* \leq \epsilon_2 + \frac{1-v_2^\epsilon}{\frac{1}{\epsilon_1-\epsilon_2} + \frac{v_2^\epsilon}{3\epsilon_2}} \tag{3.12}$$

$$\mu_1 + \frac{v_2^\mu}{\frac{1}{\mu_2-\mu_1} + \frac{1-v_2^\mu}{3\mu_1}} \leq \mu^* \leq \mu_2 + \frac{1-v_2^\mu}{\frac{1}{\mu_1-\mu_2} + \frac{v_2^\mu}{3\mu_2}} \tag{3.13}$$

where, for each property, the subscript 2 refers to the material with the higher property (for instance, if particles have higher permittivity than matrix then $\epsilon_2 = \epsilon_p$, $v_2^\epsilon = v_p$ and $\epsilon_1 = \epsilon_m$).

3.4.3 Limitations

To visualize the approximations given by the bounds, we plot two graphs. In the first one, given in Figure 3.2, we show the evolution of the bounds with respect to the volume fraction of the particles. We use the following relative electric permittivity as test parameters: $\epsilon_{r,m} = 1$, $\epsilon_{r,p} = 10$. In the second plot, given in Figure 3.3, we show the variation of the the ratio $\frac{\epsilon_p}{\epsilon_m}$ for $\epsilon_{r,m} = 1$ and a volume fraction of particles $v_p = 0.5$.

We observe that the bounds give a range that increases as the difference between ϵ_m and ϵ_p increases. Although tighter, Hashin and Shtrikman bounds still give a wide range for large differences in material properties. Hence, these bounds are clearly not handy when a composite made with large difference in properties is studied. Moreover they don't take into account for the microstructure of the composite. For instance they are independent of the shape or size of the particles.

Next, we propose a numerical method to estimate more accurately the effective electromagnetic properties. It takes the microstructure of the composite into account.

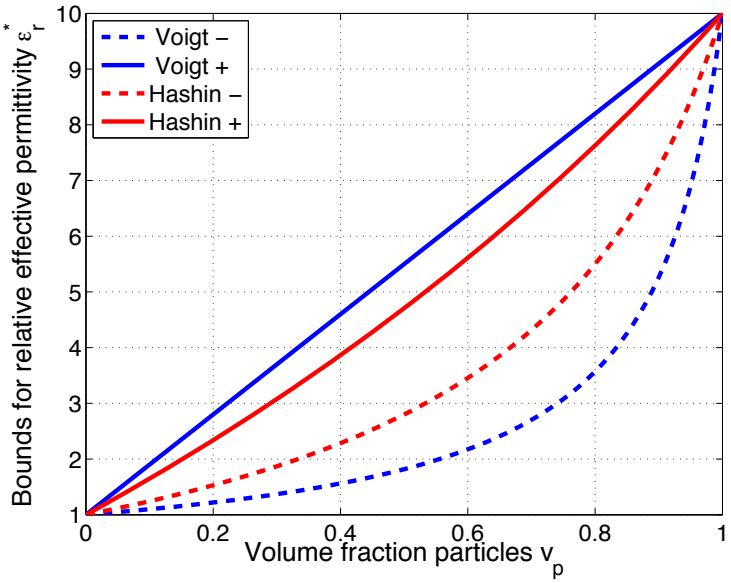

Figure 3.2: Evolution of the analytical bounds versus particle volume fractions for the test case with $\epsilon_{r,m} = 1$ and $\epsilon_{r,m} = 10$.

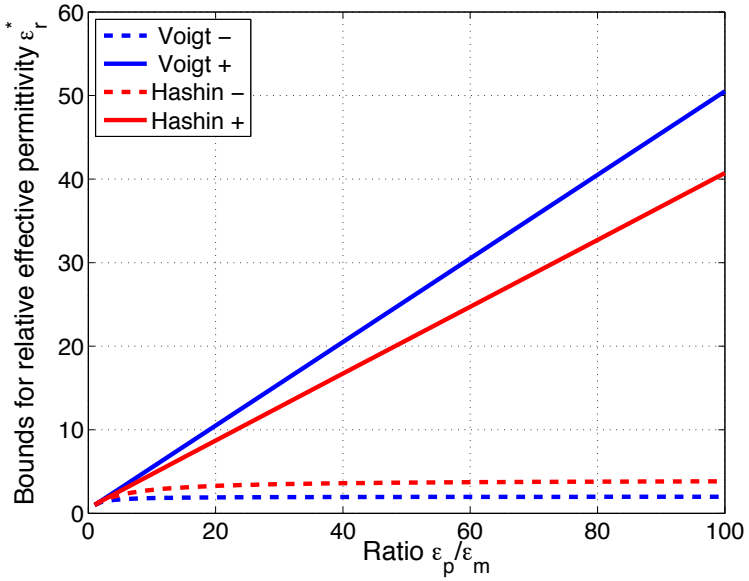

Figure 3.3: Evolution of the analytical bounds versus $\frac{\epsilon_p}{\epsilon_m}$ for for $\epsilon_{m,r} = 1$ and $v_p = 0.5$.

Chapter 4

Numerical estimation of effective electromagnetic properties

The proposed numerical method to estimate the effective electric permittivity ϵ^* and the effective magnetic permeability μ^* of a particle doped material is presented in this section. Knowing the microstructure of the envisioned particle doped composite (constituents volume fraction, particles geometry) and the electromagnetic properties of matrix and particles, this method would allow to estimate the effective electromagnetic properties of the composite. The overall method is presented first. Then, a boundary value problem is slowly built by describing the domain used, the equations considered, the numerical implemented to solve them and the boundary conditions applied. A detailed flow chart of the method is given. Finally some test simulations and results are shown to validate the method.

4.1 Overall method

The overall method to estimate the effective electromagnetic properties numerically consists of building a numerical sample of the composite material of interest, imposing some electromagnetic field at its interface, then solving over it Maxwell's equations numerically to get its electromagnetic response. The fields are then averaged appropriately to estimate the effective properties using their definition given in 3.4 and 3.8. An illustrative flowchart of the method is presented in Figure 4.1. A detailed explanation of each steps involved in the method is given in the next sections.

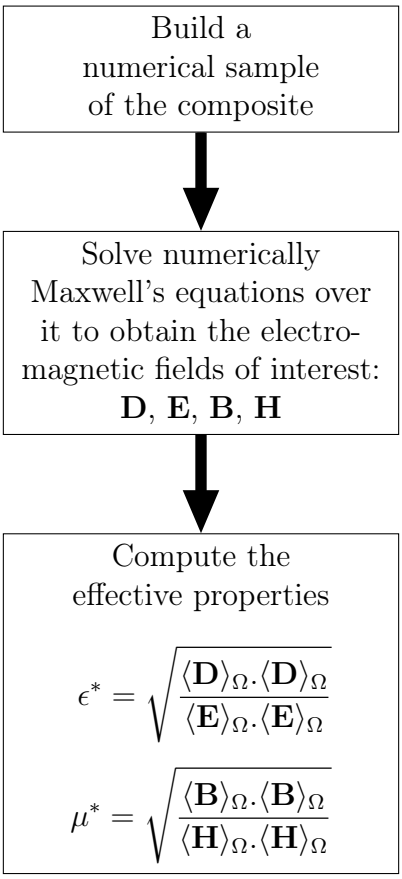

Figure 4.1: Flowchart of the overall method to estimate the effective electromagnetic properties ϵ^* and μ^* numerically.

4.2 Representative volume element

4.2.1 Definition

Solving Maxwell's equations numerically using any techniques would require some type of meshing of a sample of the particle doped composite of interest. To take the microstructure into account properly, a fine enough mesh would be required to capture the particles. This is illustrated in Figure 4.2. For instance, for a composite with spherical particles, a general rule of thumb is that a mesh size of a tenth of a particle diameter is necessary to accurately capture the presence of a particle numerically. Due to the scale difference between the overall composite - in the μm to mm range - and the particles - diameter in the nm to μm range - this would result in an enormous amount of degrees of freedom to solve for. For instance, let's assume we are using a regular cubic grid. For a particle of size $1\mu m$, a mesh size of $0.1\mu m$ would be adequate, resulting for an overall composite of dimension $1mm^3$ in a total number of $(10^4)^3 = 10^{12}$ nodes!

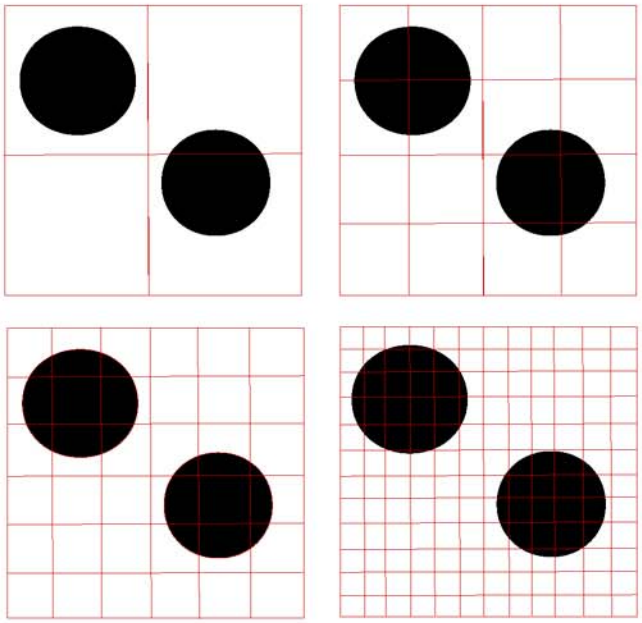

Figure 4.2: Schematic of mesh refinement around particles. Clearly a fine enough mesh is required to incorporate accurately the presence of the particles.

To overcome this problem the notion of representative volume element (RVE) has been introduced. Basically a RVE could be seen as a small representative piece of the actual composite material. It is small enough so that efficient computation could be carried, but big enough to properly represent the microstructure. A schematic of the different scale involved is shown in Figure 4.3. In order for the calculation made at the micro level to be valid at the macroscale, the RVE must satisfy certain conditions:

- It should be small enough to be assimilated as a continuum material point so that the effective property estimated over it can be assimilated as a material point property: $l \ll L$.
- It should be big enough so that the microstructure of the composite is properly captured in order for the estimated effective properties to be independent of the microstructural variations i.e. RVE independent: $l \gg d$.

Additionally, it should have the same volume fraction of both materials as in the actual composite to represent it properly. Also, the particles must be randomly distributed in order to simulate isotropic nature of the composite (no distinctive direction). More explanation on the RVE and its size requirement could be found in [20] and [5].

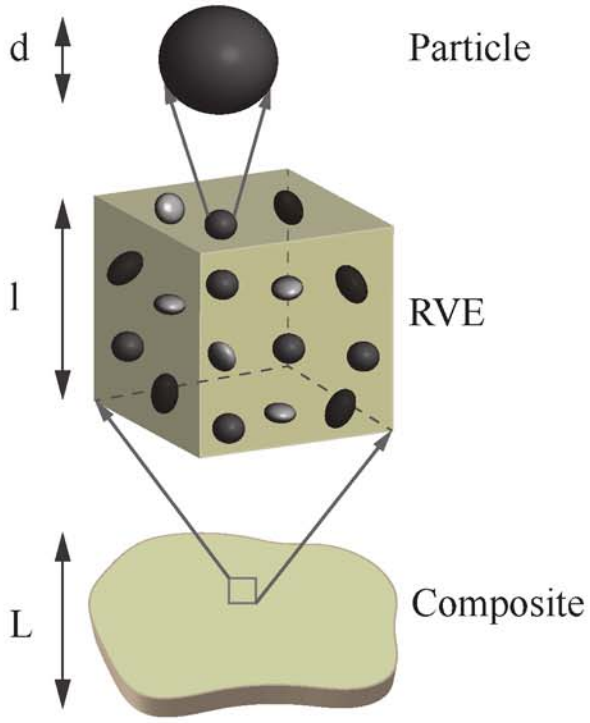

Figure 4.3: Different scales involved in RVE size estimation.

4.2.2 Numerical size estimation

The conditions mentioned previously provide only vague indications on the size of the RVE, without giving quantitative dimensions. The usual way to estimate the appropriate size is to start with an arbitrary initial size, estimate effective properties over it, then increase the size and repeat until the results stop varying significantly. This can be exposed as following:

1. Start with a RVE of size l big enough to satisfy $l \gg d$ and estimate effective property denoted P_0^* over it.

2. Increase the size of the RVE and estimate again effective property over it denoted now P_1^*.

3. Repeat until the difference between RVE q and $q-1$ fall within a chosen tolerance

$$\frac{P_q^* - P_{q-1}^*}{P_{q-1}^*} \leq tol_S \tag{4.1}$$

4. The RVE for which convergence within the required tolerance is obtained is then considered to be the appropriate size. Results over it are considered to be the final results.

4.2.3 Averaging

For each size l during the size estimation process, computation of effective properties over several random RVEs is necessary to take into account for the randomness of the repartition of the particles inside the actual composite. The average effective properties are then considered for size convergence analysis. The average effective property P^* over M random RVEs samples of a specified size l is defined as

$$P^*_{M,l} = \frac{1}{M} \sum_{k=1}^{M} P^*_{k,l} \tag{4.2}$$

No actual condition is prescribed on the number M of RVEs to consider. The bigger it is, the better randomness of the particle repartition in the actual composite would be taken into account. Evaluation over each RVE is an independent process that is parallelized in the proposed method for improved performance. Computation over up to M_c number of RVEs is conducted simultaneously, where M_c would be set based on the number of cores and processors available.

4.3 Numerical method for Maxwell's equations

We now focus on the equations we have to consider to estimate the electromagnetic fields of interests and discuss about the numerical scheme we use to solve them.

4.3.1 Equations of interest

Let designate by Ω the total volume of the RVE that is considered. Let Ω_m be the volume of matrix material and Ω_p the volume of the particles, such that $\Omega = \Omega_m \cup \Omega_p$. Also, let's designate by Γ any particle/matrix interface. This is illustrated in Figure 4.4.

Based on the discussions in section 2.8, the system of equations governing the electro-

magnetic field we have to consider over our RVE is as follow

$$\text{In } \Omega_m \cup \Omega_p :$$

$$\frac{\partial (\epsilon \mathbf{E})}{\partial t} + \sigma \mathbf{E} = \nabla \times \mathbf{H} \tag{4.3}$$

$$\frac{\partial (\mu \mathbf{H})}{\partial t} = -\nabla \times \mathbf{E} \tag{4.4}$$

$$\text{at } \Gamma :$$

$$\mathbf{n} \times (\mathbf{E}^{(m)} - \mathbf{E}^{(p)}) = \mathbf{0} \tag{4.5}$$

$$\mathbf{n} \times (\mathbf{H}^{(m)} - \mathbf{H}^{(p)}) = \mathbf{0} \tag{4.6}$$

$$\left((\epsilon \mathbf{E})^{(m)} - (\epsilon \mathbf{E})^{(p)}\right) \cdot \mathbf{n} = 0 \tag{4.7}$$

$$\left((\mu \mathbf{H})^{(m)} - (\mu \mathbf{H})^{(p)}\right) \cdot \mathbf{n} = 0 \tag{4.8}$$

where the unit normal $\mathbf{n}$ at Γ is oriented from Ω_p to Ω_m (particles to matrix).

These coupled partial differential equation are obviously not solvable analytically over a random RVE. Thus, we present a numerical method to solve them.

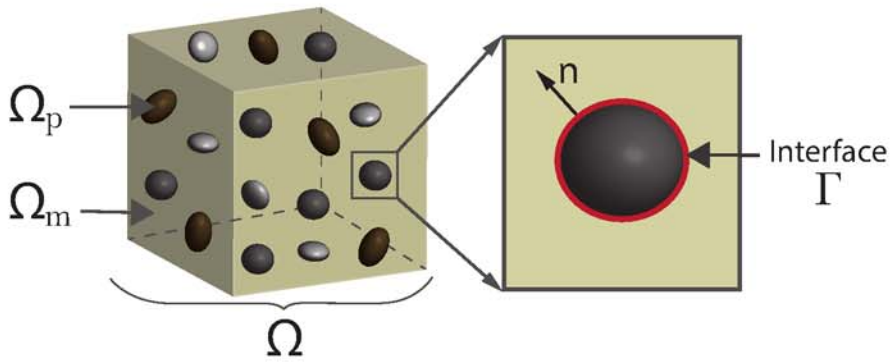

Figure 4.4: Domain repartition on a RVE.

4.3.2 Yee's scheme

Yee's scheme [31] is implemented to solve the previous system of equations. The advantages of this method are its second order accuracy in time and space. Moreover, its explicit format in time makes it very efficient computationally. It also satisfies exactly the divergence equation once they are set initially. A meticulous explanation on the method and general

computational electrodynamics discussions are available in [25] and [19].

This finite difference scheme uses a particular discretization where alternation in space and time occurs between the components of **E** and **H**. The spatial discretization in 3D is made using the so-called Yee's cell that is presented in Figure 4.5.

For the rest of the dissertation, we call Δx, Δy, and Δz the spatial discretization step size in direction x, y and z, respectively. Let Δt be the temporal discretization size. We introduce for any function $f(x, y, z, t)$ the notation $f^n_{i,j,k} = f(i\Delta x, i\Delta y, i\Delta z, n\Delta t)$.

The following discretization of equations 4.3 and 4.4 are used in Yee's scheme

$$\begin{aligned} H_x|^{n+\frac{1}{2}}_{i,j+\frac{1}{2},k+\frac{1}{2}} =& H_x|^n_{i,j+\frac{1}{2},k+\frac{1}{2}} + \frac{\Delta t}{\mu_{i,j+\frac{1}{2},k+\frac{1}{2}}} \left(\frac{E_y|^n_{i,j+\frac{1}{2},k+1} - E_y|^n_{i,j+\frac{1}{2},k}}{\Delta z} \right. \\ & \left. - \frac{E_z|^n_{i,j+1,k+\frac{1}{2}} - E_z|^n_{i,j,k+\frac{1}{2}}}{\Delta y} \right) \end{aligned} \tag{4.9}$$

$$\begin{aligned} H_y|^{n+\frac{1}{2}}_{i+\frac{1}{2},j,k+\frac{1}{2}} =& H_y|^n_{i+\frac{1}{2},j,k+\frac{1}{2}} + \frac{\Delta t}{\mu_{i+\frac{1}{2},j,k+\frac{1}{2}}} \left(\frac{E_z|^n_{i+1,j,k+\frac{1}{2}} - E_z|^n_{i,j,k+\frac{1}{2}}}{\Delta x} \right. \\ & \left. - \frac{E_x|^n_{i+\frac{1}{2},j,k+1} - E_x|^n_{i+\frac{1}{2},j,k}}{\Delta z} \right) \end{aligned} \tag{4.10}$$

$$\begin{aligned} H_z|^{n+\frac{1}{2}}_{i+\frac{1}{2},j+\frac{1}{2},k} =& H_z|^n_{i+\frac{1}{2},j+\frac{1}{2},k} + \frac{\Delta t}{\mu_{i+\frac{1}{2},j+\frac{1}{2},k}} \left(\frac{E_x|^n_{i+\frac{1}{2},j+1,k} - E_x|^n_{i+\frac{1}{2},j,k}}{\Delta y} \right. \\ & \left. - \frac{E_y|^n_{i+1,j+\frac{1}{2},k} - E_y|^n_{i,j+\frac{1}{2},k}}{\Delta x} \right) \end{aligned} \tag{4.11}$$

$$E_x|^{n+1}_{i+\frac{1}{2},j,k} = \frac{2\epsilon_{i+\frac{1}{2},j,k} - \sigma_{i+\frac{1}{2},j,k}\Delta t}{2\epsilon_{i+\frac{1}{2},j,k} + \sigma_{i+\frac{1}{2},j,k}\Delta t} E_x|^{n}_{i+\frac{1}{2},j,k} + \frac{2\Delta t}{2\epsilon_{i+\frac{1}{2},j,k} + \sigma_{i+\frac{1}{2},j,k}\Delta t} \left(\frac{H_z|^{n+\frac{1}{2}}_{i+\frac{1}{2},j+\frac{1}{2},k} - H_z|^{n+\frac{1}{2}}_{i+\frac{1}{2},j-\frac{1}{2},k}}{\Delta y} - \frac{H_y|^{n+\frac{1}{2}}_{i+\frac{1}{2},j,k+\frac{1}{2}} - H_y|^{n+\frac{1}{2}}_{i+\frac{1}{2},j,k-\frac{1}{2}}}{\Delta z} \right) \tag{4.12}$$

$$E_y|^{n+1}_{i,j+\frac{1}{2},k} = \frac{2\epsilon_{i,j+\frac{1}{2},k} - \sigma_{i,j+\frac{1}{2},k}\Delta t}{2\epsilon_{i,j+\frac{1}{2},k} + \sigma_{i,j+\frac{1}{2},k}\Delta t} E_y|^{n}_{i,j+\frac{1}{2},k} + \frac{2\Delta t}{2\epsilon_{i,j+\frac{1}{2},k} + \sigma_{i,j+\frac{1}{2},k}\Delta t} \left(\frac{H_x|^{n+\frac{1}{2}}_{i,j+\frac{1}{2},k+\frac{1}{2}} - H_x|^{n+\frac{1}{2}}_{i,j+\frac{1}{2},k-\frac{1}{2}}}{\Delta z} - \frac{H_z|^{n+\frac{1}{2}}_{i+\frac{1}{2},j+\frac{1}{2},k} - H_z|^{n+\frac{1}{2}}_{i-\frac{1}{2},j+\frac{1}{2},k}}{\Delta x} \right) \tag{4.13}$$

$$E_z|^{n+1}_{i,j,k+\frac{1}{2}} = \frac{2\epsilon_{i,j,k+\frac{1}{2}} - \sigma_{i,j,k+\frac{1}{2}}\Delta t}{2\epsilon_{i,j,k+\frac{1}{2}} + \sigma_{i,j,k+\frac{1}{2}}\Delta t} E_z|^{n}_{i,j,k+\frac{1}{2}} + \frac{2\Delta t}{2\epsilon_{i,j,k+\frac{1}{2}} + \sigma_{i,j,k+\frac{1}{2}}\Delta t} \left(\frac{H_y|^{n+\frac{1}{2}}_{i+\frac{1}{2},j,k+\frac{1}{2}} - H_y|^{n+\frac{1}{2}}_{i-\frac{1}{2},j,k+\frac{1}{2}}}{\Delta x} - \frac{H_x|^{n+\frac{1}{2}}_{i,j+\frac{1}{2},k+\frac{1}{2}} - H_x|^{n+\frac{1}{2}}_{i,j-\frac{1}{2},k+\frac{1}{2}}}{\Delta y} \right) \tag{4.14}$$

It is important to mention that Yee's scheme converges to the actual solution only when the CFL condition is met, which translate into the following restriction on the time step

$$\Delta t_{Yee} \leq \Delta t_{CFL} = \frac{\min(\Delta x, \Delta y, \Delta z)}{\sqrt{3} c_{max}} \tag{4.15}$$

where c_{max} =max$\{c_p, c_m\}$, with $c_p = \frac{1}{\sqrt{\mu_p \epsilon_p}}$ and $c_m = \frac{1}{\sqrt{\mu_m \epsilon_m}}$ being respectively the velocity of the wave in the particles and the matrix material.

4.3.3 Problems at material interfaces

In Yee's scheme, material properties can be specified only at each nodes of the cells. Hence, the particles are approximated with a step like shape as shown in Figure 4.6. The interface conditions 4.5 to 4.8 are then enforced automatically on this approximation. This will introduce an error known as stair case error [8] as the numerical solution would be obtained for a stepped particle instead of a spherical particle. Novel numerical schemes have been introduced to overcome this problem, as in [4] and [1]. They usually involve changing the coefficients for nodes near the actual material interface in order to reduce the error. However their implementation could be arduous and they often lose ease of setup and computational efficiency provided by Yee's scheme.

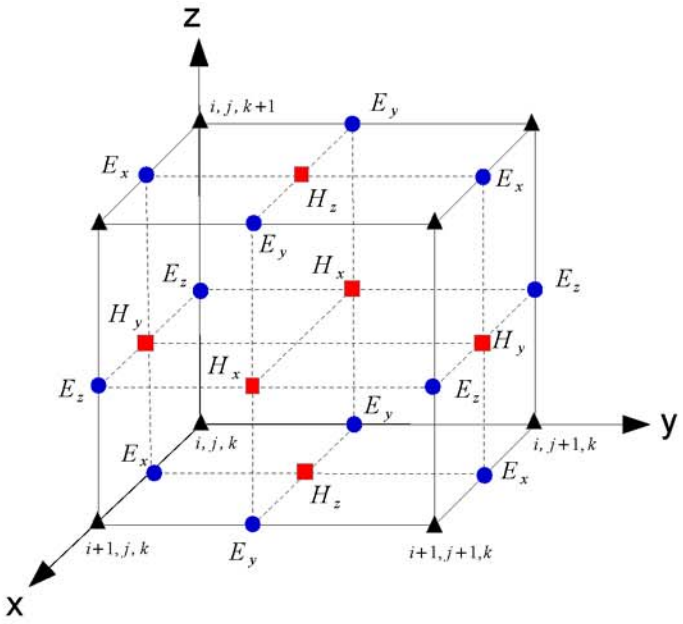

Figure 4.5: Schematic of a Yee cell.

From an engineering point of view we can deal with this problem in two ways. We can assume that particles are not going to be properly spherical in the actual material, due to manufacturing errors, and live up with the stair case approximation. It is also possible to assume that there is no hard jump in properties in the actual composite but rather a smooth variation due to built up material at the interface that is a mix of matrix and particle material. This is taken into account numerically by using Laplacian property smoothing [34] at the interface, where any property P is replaced by a smooth spatial representation P^S as

$$P^S_{i,j,k} = \frac{1}{6}\left(P_{i+1,j,k} + P_{i-1,j,k} + P_{i,j+1,k} + P_{i,j-1,k} + P_{i,j,k+1} + P_{i,j,k-1}\right) \tag{4.16}$$

This omits the presence of hard jump in material properties at material interface, and remove the requirement to take into account for interface conditions. We implement both possibilities here and comparison in the results is done in section 4.5.

4.3.4 Boundary conditions on RVE

Yee's scheme requires to specify on the RVE initial conditions for **E** and **H**, and boundary conditions for three of the six total components of **E** and **H** combined. Initial condition is simply a no field state. The boundary conditions are required to satisfy certain condition in order for the results computed on the RVE to be valid on the actual macroscale composite. This is derived by imposing energy conservation between the two scales as explained originally in [11] for mechanics and extended to electromagnetism in [32]. It is shown that boundary

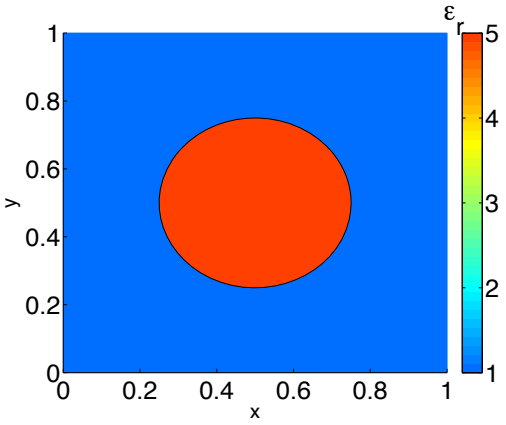

(a) Ideal interface

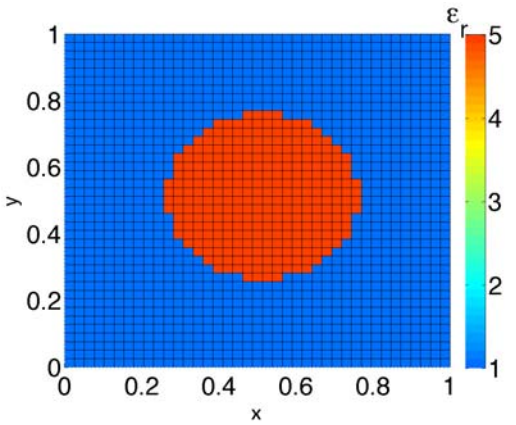

(b) Stair case approximation in Yee's cell

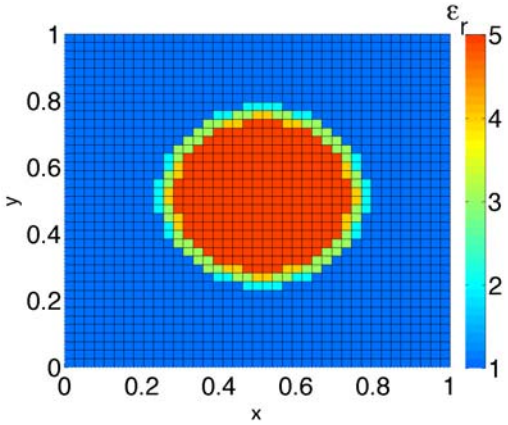

(c) Property smoothing near interface

Figure 4.6: Illustration of ideal and approximated particle/matrix interface for a matrix with $\epsilon_{r,m} = 1$ and particle with $\epsilon_{r,p} = 5$.

conditions linearly growing in time satisfy this condition and are used here. We impose boundary conditions on the components of **E** by locating them on the outer side on the Yee's cell having an interface at the boundary. Boundary values are increased at slow linear rate in order to avoid introduction of oscillating fields. Notice that the magnitude of the boundary conditions should not influence the final estimation of the effective properties that are supposed to be constants of the composite.

4.4 Detailed flowchart

A detailed flowchart of the numerical method is given in Figure 4.7. First, composite parameters are specified: number of phases, material properties, material volume fractions and the shape of particles. Then, a starting number of particles N_p is indicated, and the

associate RVE size l required to satisfy the specified volume fractions is determined by $l = \left(\frac{N_p \Omega_p}{v_p}\right)^{\frac{1}{3}}$. As mentioned previously, estimations of effective electromagnetic properties over several RVEs with random arrangement of particles (we call M total number of RVEs considered) are required to obtain statistically representative results. Computation of several RVEs is done in parallel fashion: up to M_c computations are carried out simultaneously. The RVEs are divided into Yee cells, and the **E** and **H** fields are computed over each by solving Maxwell's equations using Yee's scheme based on specified boundary conditions. Constitutive laws are used simultaneously to compute the **D** and **B** fields. At each time step these fields are averaged over the considered RVE in order to compute ϵ^* and μ^*. When their values become steady, the process is stopped. Once results over all M number of RVEs are available, they are averaged. We then increase N_p while keeping volume fractions v_p fix, to obtain RVEs of bigger size. The process is stopped when difference in the average effective properties over two successive sizes vary within a specified tolerance, tol_S.

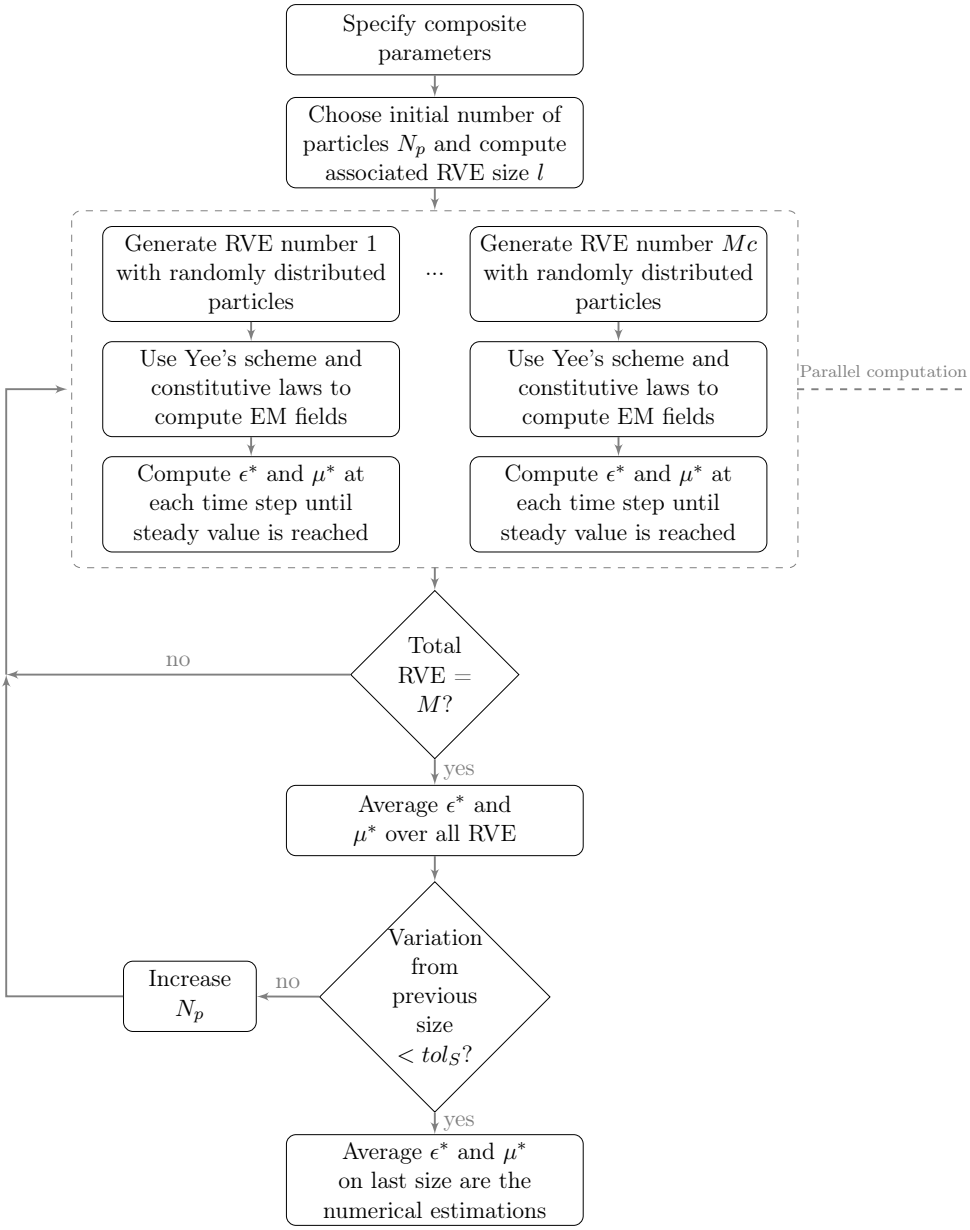

Figure 4.7: Flowchart of the overall numerical method proposed to estimate the effective electromagnetic properties.

4.5 Simulation and results

4.5.1 Validation with analytical bounds

We check first the validity of the proposed numerical method by verifying that the results on a model problem fall between the corresponding analytical bounds. A two-phase com-

posite is considered, made of matrix and spherical non-overlapping particles. The following parameters are used

1. Matrix properties
   - Relative electric permittivity $\epsilon_{r,m} = 1$
   - Relative magnetic permeability $\mu_{r,m} = 1$
   - Electric conductivity $\sigma_m = 0\ S/m$

2. Particles properties
   - Relative electric permittivity $\epsilon_{r,p} = 10$
   - Relative magnetic permeability $\mu_{r,p} = 5$
   - Electric conductivity $\sigma_p = 0\ S/m$

3. RVE parameters
   - Particle diameter $d = 2\mu m$
   - Total number of RVEs is $M = 30$
   - Simultaneous computation over $M_C = 8$ RVEs
   - Number of particles $N_p = 50$ initially, then increased by 50 until convergence criteria is met
   - Tolerance on size $tol_S = 3\%$
   - Volume fraction of particle v_p is varied to obtain different results
   - The RVE size is then chosen such that $l = \left(\frac{N_p(4/3)\pi(d/2)^3}{v_p}\right)^{\frac{1}{3}}$

4. Numerical solver parameters
   - Mesh size $\Delta x = \Delta y = \Delta z = \frac{d}{10}$
   - $\Delta t = \Delta t_{CFL}$

5. Electromagnetic field
   - Electric field: $\mathbf{E} = (0, 0, 0)\ V/m$ at $t = 0$ and linearly growing with time on the side of the RVE with normal $\mathbf{e}_y$ and $-\mathbf{e}_y$ until $\mathbf{E} = (1000, 1000, 1000)\ V/m$ over 1000 time step
   - Magnetic field: $\mathbf{H} = 0\ A/m$ at $t = 0$

Materials with fairly close electromagnetic properties are used on purpose in order to have tighter range in the bounds and validate the method properly. We considered cases with and without property smoothing at matrix/particles interface in order to test the validity of both. Multiple results are presented next.

In Figure 4.8 the evolution of ϵ_r^* and μ_r^* for one RVE is shown. The parameters used are $N_p = 200$ particles and $v_p = 0.2$. We see that the effective properties values vary at first as the fields settle, then reach a steady value. The result with properties smoothing fall in between the bounds for both ϵ_r^* and μ_r^*. We notice that the result without smoothing fall outside the Hashin-Shtrikman bounds for μ_r^* where the bounds are tighter.

Once a steady value is captured for the effective properties the simulation is stopped. We move on to the next RVE of the same size. The results over 30 randomly generated RVE of same size are shown in Figure 4.9. The results vary within a range that is very narrow and a better estimation than the bounds is obtained.

The evolution of the relative effective properties averaged over 30 RVEs for different RVE size is shown in Figure 4.10. The initial sample has parameters $N_p = 50$, $v_p = 0.2$. Then N_p is increased keeping v_p constant in order to obtain bigger RVE size l. We observe that a certain convergence in numerically estimated effective properties occur for a RVE with $N_p = 200$ particles in this particular case.

Finally we show in Figure 4.11 evolution of average effective properties for different volume fraction of particles v_p.

The material parameters were intentionally chosen to obtain a very small range for the Hashin-Shtrikman bounds. We observe that results without smoothing fail to pass the bounds test in the case of μ_r^*, which has very tight bounds. On the other hand, all of the results with smoothing successfully fall inside those bounds. Hence, the property smoothing technique is used for all the simulations next.

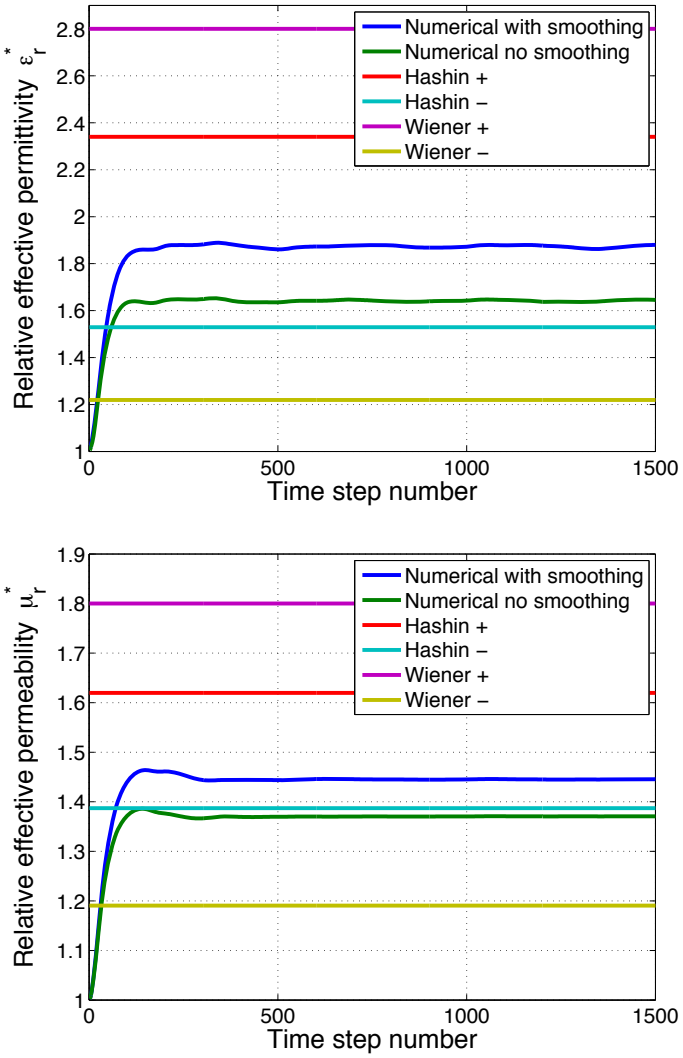

Figure 4.8: Evolution of the relative effective electric permittivity ϵ_r^* (top) and relative effective magnetic permeability μ_r^* (bottom) versus time step number for one simulation, along with analytical bounds.

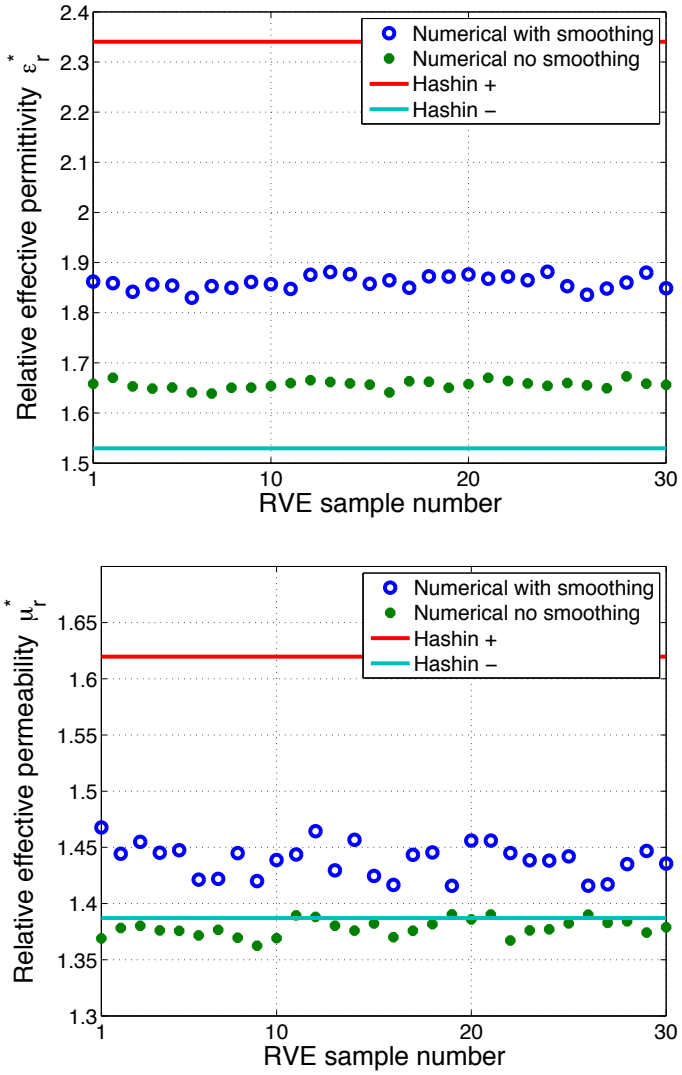

Figure 4.9: Relative effective electric permittivity ϵ_r^* (top) and relative effective magnetic permeability μ_r^* (bottom) over different random RVE of similar size, along with analytical bounds.

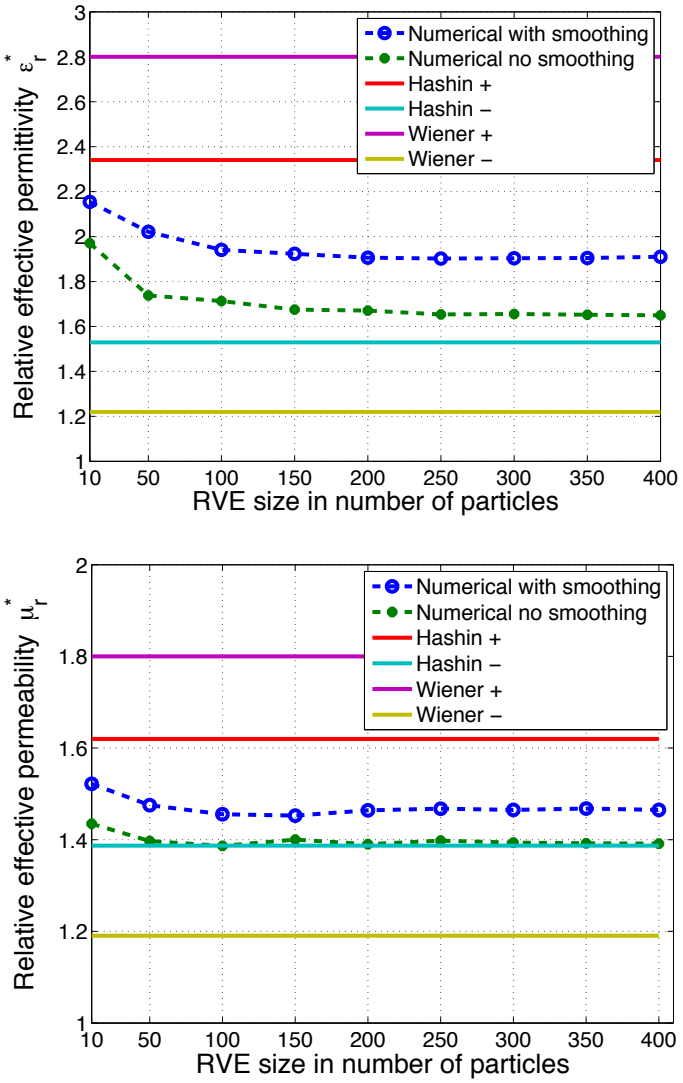

Figure 4.10: Evolution of average relative effective electric permittivity ϵ_r^* (top) and relative effective magnetic permeability μ_r^* (bottom) over different size RVE, along with analytical bounds.

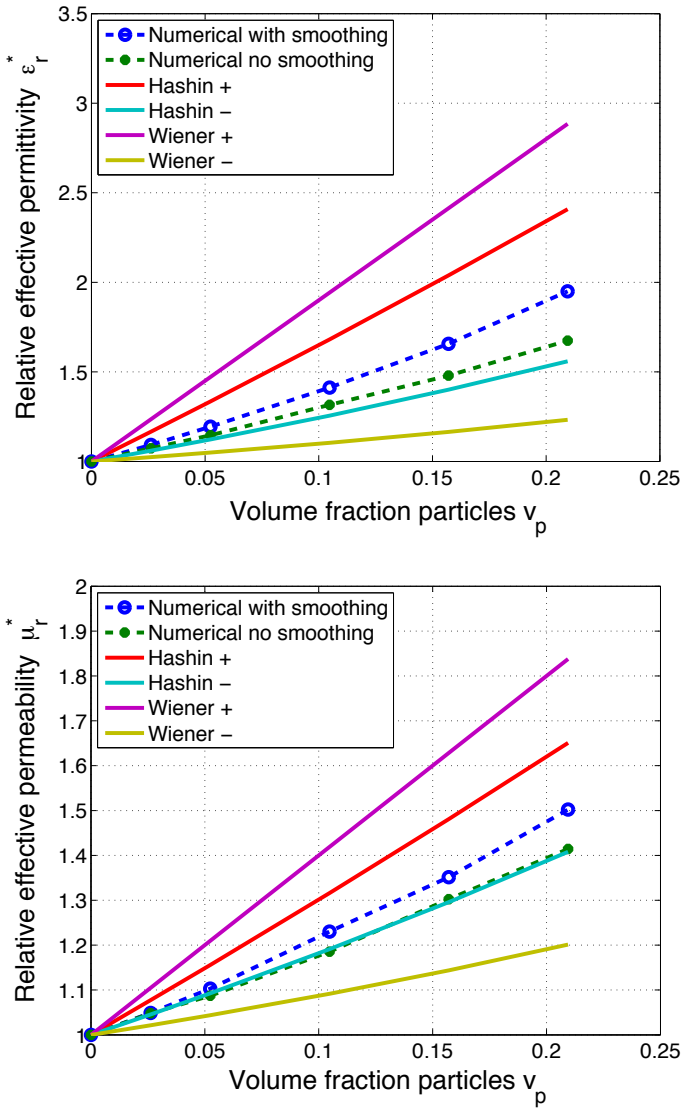

Figure 4.11: Evolution of average relative effective electric permittivity ϵ_r^* (top) and relative effective magnetic permeability μ_r^* (bottom) for different volume fraction of particles, along with analytical bounds.

4.5.2 Comparison with experimental results

Experimental estimations for the effective electric permittivity of a composite made by doping polyethylene (PE) with $BaTiO_3$ particles are presented in [26]. The results provided are used to observe the accuracy of the proposed numerical method. The following parameters are specified in [26]

1. PE
   - Relative electric permittivity $\epsilon_{r,m} = 2.5$
2. $BaTiO_3$
   - Particle size $d \approx 100\mu m$
   - Relative electric permittivity $\epsilon_{r,p} = 72.5$

All other parameters are similar to previous the section. Numerical computation of the effective electric permittivity is conducted using these parameters. Comparison between experimental and numerical results is shown in Figure 4.12. We observe better estimation than analytical bounds. However, difference in the results is still noticeable, especially at higher volume fraction. This could be due to several factors. We list the most prominent below:

- the property smoothing technique provides only an approximation without taking actually into account exactly for the particles' spherical shape, this could introduce errors in computing the effective properties,
- external factors such as temperature variation could influence the results but is not taken into accounting in the numerical model,
- the particle size provided in [26] is only approximate, it is possible that variable size particles were used in the experiment.

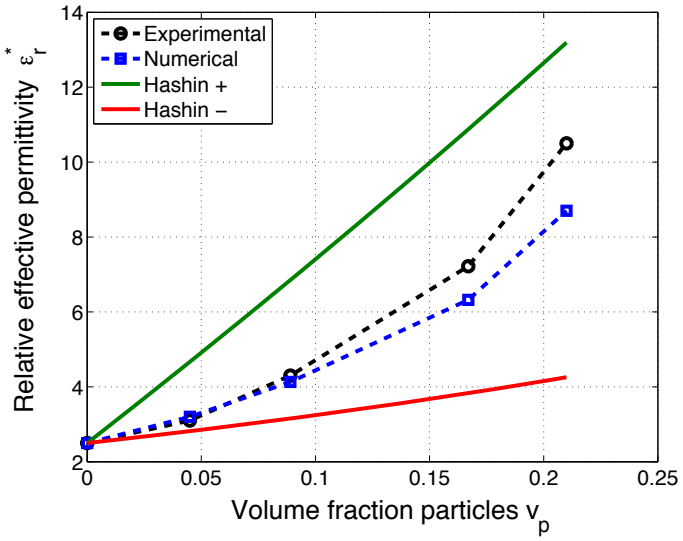

Figure 4.12: Evolution of the numerical effective electric permittivity ϵ_r^* along with analytical bounds and experimental results from [26].

4.5.3 Particle size influence

In this section influence of particle size on the effective electromagnetic properties is assessed. To do so, the following parameters are used

1. Matrix material properties
   - Relative electric permittivity $\epsilon_{r,m} = 1$
   - Relative magnetic permeability $\mu_{r,m} = 1$
   - Electric conductivity $\sigma_m = 0\ S/m$
2. Particles material properties
   - Relative electric permittivity $\epsilon_{r,p} = 70$
   - Relative magnetic permeability $\mu_{r,p} = 40$
   - Electric conductivity $\sigma_p = 0\ S/m$
3. RVE parameters
   - Particle diameter is varied
   - Total number of RVEs is $M = 30$
   - Simultaneous computation over $M_C = 8$ RVEs

- Number of particles $N_p = 200$
- Volume fraction of particle $v_p = 0.2$
- The RVE size is then chosen such that $l = \left(\frac{N_p(4/3)\pi(d/2)^3}{v_p}\right)^{\frac{1}{3}}$

4. Numerical solver parameters

   - Mesh size $\Delta x = \Delta y = \Delta z = \frac{d}{10}$
   - $\Delta t = \Delta t_{CFL}$

5. Electromagnetic field

   - Electric field: $\mathbf{E} = (0, 0, 0)\ V/m$ at $t = 0$ and linearly growing with time on the side of the RVE with normal $\mathbf{e}_y$ and $-\mathbf{e}_y$ until $\mathbf{E} = (1000, 1000, 1000)\ V/m$ over 1000 time step
   - Magnetic field: $\mathbf{H} = 0\ A/m$ at $t = 0$

We show in Figure 4.13 the evolution of the effective properties with particles diameter varying from $5\mu m$ to $10\mu m$. We observe that, for this particular range, a bigger particle size is recommended for higher effective permittivity ϵ^*. On the other hand, a smaller particle size is recommended for higher effective permeability μ^*.

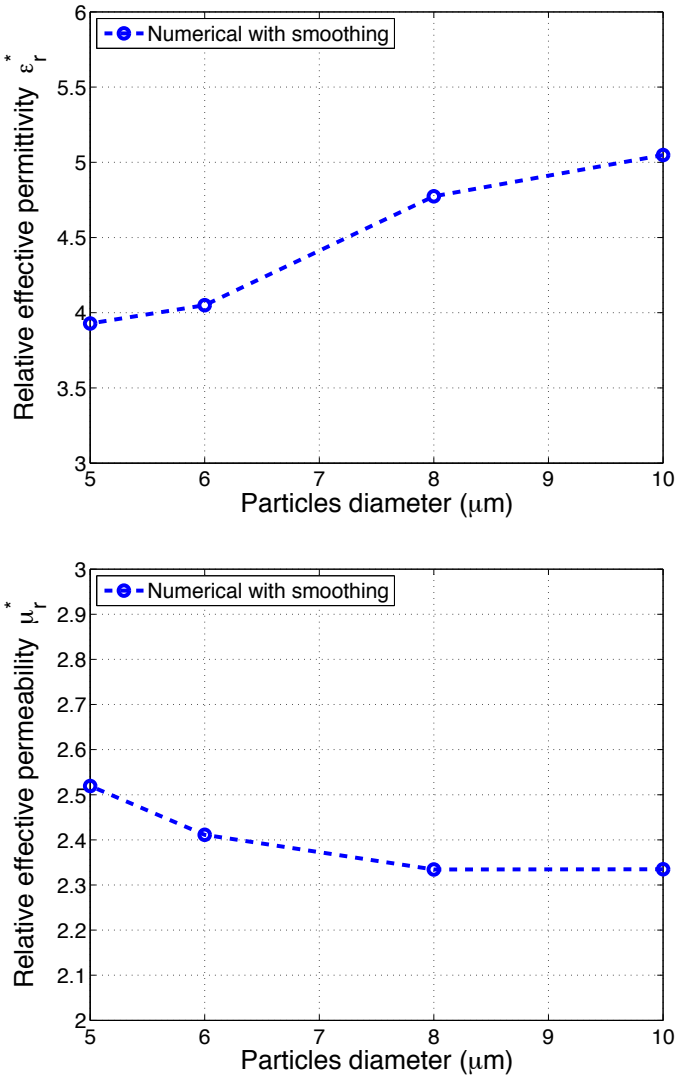

Figure 4.13: Evolution of effective electric permittivity ϵ_r^* (top) and relative effective magnetic permeability μ_r^* (bottom) for different particle size.

4.5.4 Influence of inclusions shape

Although spherical particles are preferred in the applications of interest due to ease of manufacturing at small scales, various shapes could be envisioned for the inclusions [12]. In this section, we assess the effect of different shape of ellipsoid on the effective electromagnetic properties to illustrate the capabilities of the proposed method to work with any particle shape. Ellipsoid are described by the following equations

$$\frac{(x-x_0)^2}{a^2}+\frac{(y-y_0)^2}{b^2}+\frac{(z-z_0)^2}{c^2}=1 \tag{4.17}$$

where (x_0, y_0, z_0) are the coordinates of the center of the ellipsoid, and a, b, c are the length of the semi-principal axes. The choice of ellipsoid inclusions here is based on its ability to represent variety of shape depending the selection of parameters a, b, and c. Different shapes are shown in Figure 4.14 for $a = b = r_p$ and variable values of c.

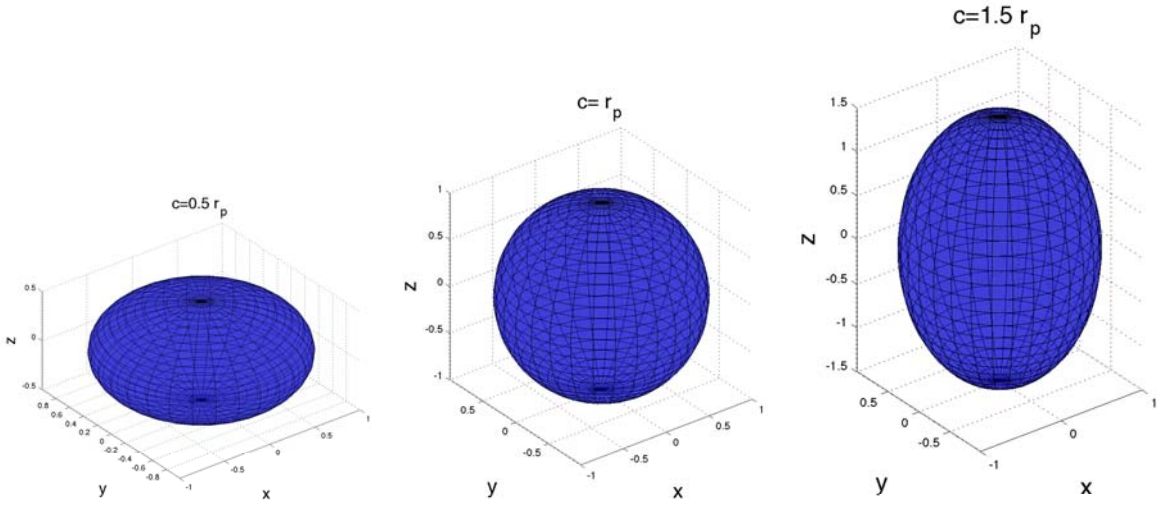

Figure 4.14: Various ellipsoids for $a = b = r_p = 1$ and variable c.

The numerical method described in the flow chart 4.7 is applied to different shape of ellipsoid, and effective electromagnetic properties are computed for each of them. The parameters a, b and the volume fraction of inclusion v_p are kept constant. Results are computed for different values of c. Random orientation of all 3 axis is imposed for each ellipsoid added to an RVE in order to obtain random orientation and simulate overall isotropy and randomness in the actual composite.

The complete list of parameters used is given below

1. Matrix material properties
   - Relative electric permittivity $\epsilon_{r,m} = 1$
   - Relative magnetic permeability $\mu_{r,m} = 1$
   - Electric conductivity $\sigma_m = 0\ S/m$

2. Particles material properties
   - Relative electric permittivity $\epsilon_{r,p} = 200$

- Relative magnetic permeability $\mu_{r,p} = 100$
- Electric conductivity $\sigma_p = 0\ S/m$

3. RVE parameters

- Ellipsoid semi-principal axis $a = b = r_p = 1\mu m$, c is varied
- Total number of RVEs is $M = 30$
- Simultaneous computation over $M_C = 8$ RVEs
- Number of particles $N_p = 200$
- Volume fraction of inclusions $v_p = 0.1$
- The RVE size is then chosen such that $l = \left(\frac{N_p(4/3)\pi abc}{v_p}\right)^{\frac{1}{3}}$

4. Numerical solver parameters

- Mesh size $\Delta x = \Delta y = \Delta z = \frac{d}{10}$
- $\Delta t = \Delta t_{CFL}$

5. Electromagnetic field

- Electric field: $\mathbf{E} = (0, 0, 0)\ V/m$ at $t = 0$ and linearly growing with time on the side of the RVE with normal $\mathbf{e}_y$ and $-\mathbf{e}_y$ until $\mathbf{E} = (1000, 1000, 1000)\ V/m$ over 1000 time step
- Magnetic field: $\mathbf{H} = 0\ A/m$ at $t = 0$

Evolution of the effective electromagnetic properties for different values of c is shown in Figure 4.15. We observe that shape influence their value. Although variations for this particular simulation are in a small range, we can see that shape other than spherical could deliver higher values. We find here that the highest value for ϵ^* is obtained for $c = 0.9r_p$ and the highest value for μ^* is obtained for $c = 0.5r_p$.

For the rest of the dissertation we consider again only spherical particles.

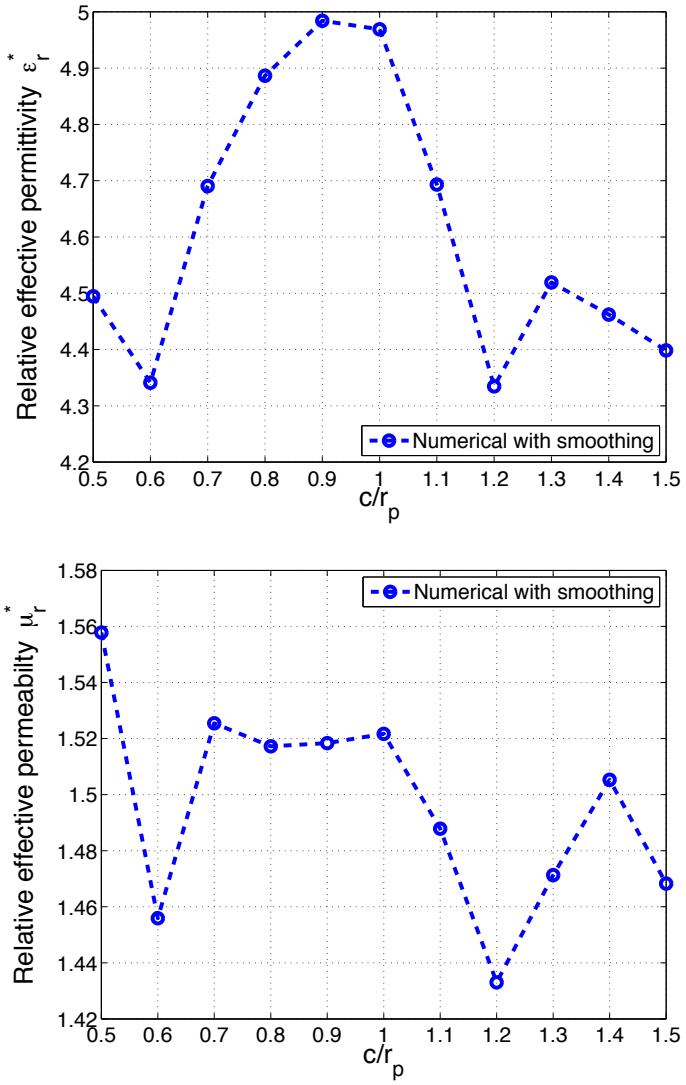

Figure 4.15: Relative effective electric permittivity ϵ_r^* (top) and relative effective magnetic permeability μ_r^* (bottom) for different ellipsoid shapes with parameters $a = b = r_p$ and variable c. Note that results for $c = r_p$ correspond to spherical particles.

Chapter 5

Thermal effects on effective electromagnetic properties

In this chapter we assess thermal dependence of the effective electromagnetic properties. The importance of thermal effects for the applications of interest is discussed first. Then, the effects of temperature on electric permittivity and magnetic permeability are explored. Finally we introduce a numerical method to predict the variation of effective electromagnetic properties with temperature.

5.1 Importance of thermal effects

For the applications of interest, namely dielectrics in capacitors and magnetic cores in planar inductors, the composite material is expected to evolve in an environment where a strong electromagnetic field is present. Thus, a temperature increase via Joule heating is to be expected [10]. It is also shown that variation in temperature affects the value of the electric permittivity ϵ and magnetic permeability μ of most materials [21], [16], [22]. Hence, we have a two way coupling as illustrated in Figure 5.1.

Temperature variation would certainly affect the properties of the individual materials a particle composite is made of, affecting subsequently its effective electromagnetic properties. Assessing the effect of temperature variation on the effective electromagnetic properties is thus key for designing a viable composite for the applications of interest. We propose here a numerical method to do so.

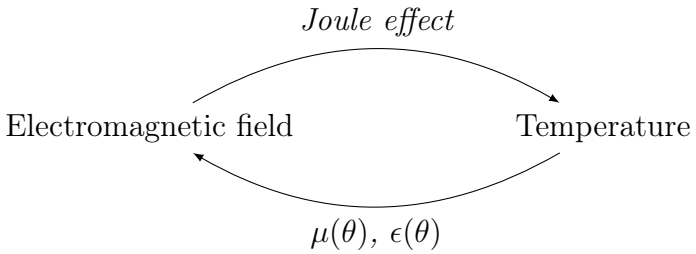

Figure 5.1: Illustration of the two way electromagnetic-thermal coupling.

5.2 Thermal dependence of electromagnetic properties

The electromagnetic properties of most materials are thermally dependent, as discussed in depth in [21] and [16] for the electric permittivity, and in [22] for the magnetic permeability. These behaviors are usually determined experimentally when required.

Generally speaking, no predictable behavior is observed: the variations are highly material dependent. Many analytical models have however been proposed, such as the one listed in [23], [17], [17], and [34].

5.3 Numerical estimation of the thermal dependency of effective electromagnetic properties

5.3.1 Overall method

We assume the variation with temperature of the electromagnetic properties of each individual material constituting the particle doped composite of interest is known either empirically or via analytical model. Then, the proposed method consists of evaluating these properties for different temperature and using for each temperature the numerical method presented in section 4.4 to evaluate the corresponding effective properties. The flow chart of the method is presented in Figure 5.2.

5.3.2 Results on test problem

We apply the method to a test problem. We assume for this that the electromagnetic properties of the matrix material are thermally independent. For simulation purposes, sigmoid type behavior for the electric permittivity and magnetic permeability of the particle material is considered [34]

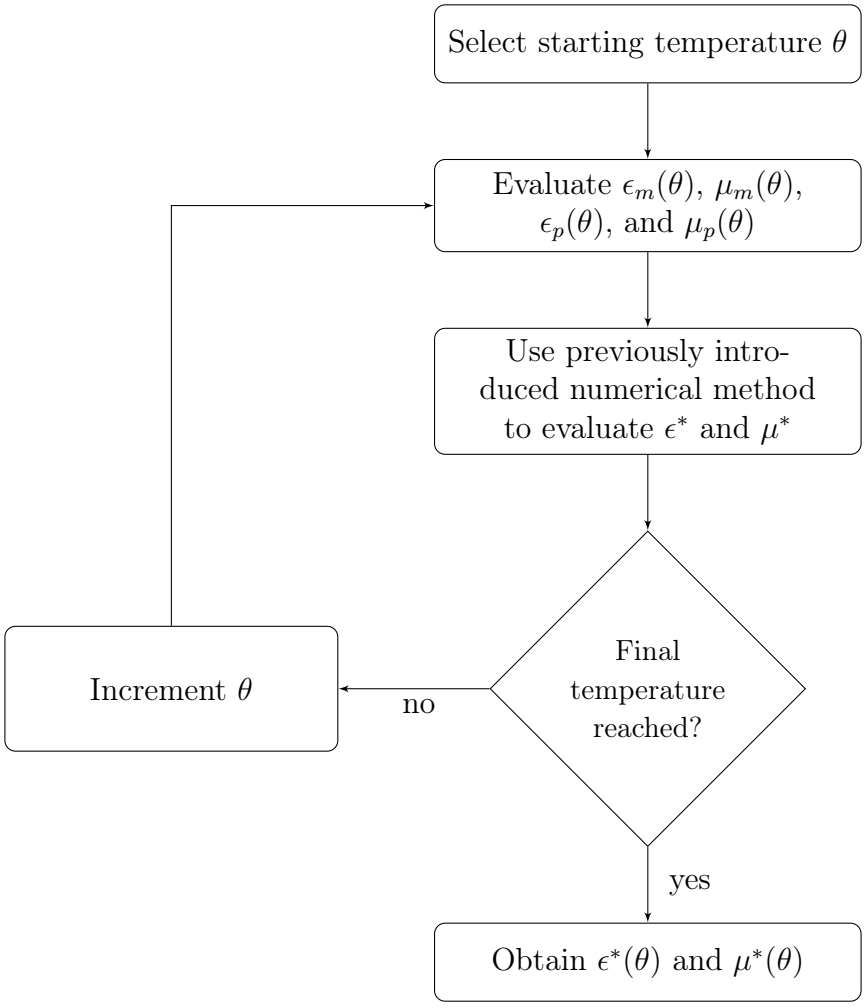

Figure 5.2: Flow chart of the numerical method to estimate thermal behavior of effective electromagnetic properties.

$$\epsilon_r(\theta) = 1 + \epsilon_r^s F_s\left(\alpha^\epsilon, \frac{\theta - \theta_0}{\theta_0}\right) \tag{5.1}$$

$$\mu(\theta) = 1 + \mu_r^s F_s\left(\alpha^\mu, \frac{\theta - \theta_0}{\theta_0}\right) \tag{5.2}$$

In this model, ϵ_r^s, α^ϵ, μ_r^s, and α^μ are assumed empirically determined material properties, θ is the current temperature, and θ_0 is a reference temperature. Here, F_s designates the sigmoid function defined by

$$F_s(\alpha, x) = \frac{1}{1 + e^{-\alpha x}} \tag{5.3}$$

An illustration of the function is given in Figure 5.3. Basically ϵ_r^s and μ_r^s are thresholds to the variation of ϵ and μ. The parameters α^ϵ and α^μ are positive for increasing property with temperature, otherwise they are negative.

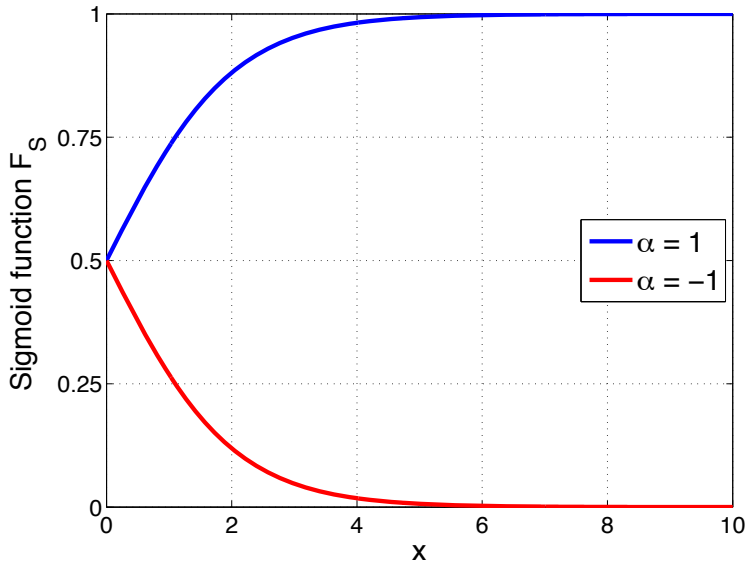

Figure 5.3: Plot of the evolution of the sigmoid function F_s for $\alpha = 1$ and $\alpha = -1$.

The following parameters are considered for the test simulation

1. Matrix material properties (assumed thermally independent)

- Relative electric permittivity: $\epsilon_{r,m} = 1$
- Relative magnetic permeability: $\mu_{r,m} = 1$
- Electrical conductivity: $\sigma_m = 0\ S/m$

2. Particles material properties

- Relative electric permittivity: $\epsilon^s_{r,p} = 38$, $\alpha^\epsilon_p = -2$
- Relative magnetic permeability: $\mu^s_{r,p} = 18$, $\alpha^\mu_p = -2.5$
- Electrical conductivity: $\sigma_p = 0\ S/m$
- Reference temperature: $\theta_0 = 303K$

3. RVE parameters

- Particle diameter $d = 2\mu m$
- Total number of RVEs is $M = 30$
- Simultaneous computation over $M_C = 8$ RVEs
- Number of particles $N_p = 200$
- Volume fraction of particle $v_p = 0.2$
- The RVE size is then chosen such that $l = \left(\frac{N_p(4/3)\pi(d/2)^3}{v_p}\right)^{\frac{1}{3}}$

4. Numerical solver parameters

- Mesh size $\Delta x = \Delta y = \Delta z = \frac{d}{10}$
- $\Delta t = \Delta t_{CFL}$

5. Electromagnetic field

- Electric field: $\mathbf{E} = (0, 0, 0)\ V/m$ at $t = 0$ and linearly growing with time on the side of the RVE with normal $\mathbf{e}_y$ and $-\mathbf{e}_y$ until $\mathbf{E} = (1000, 1000, 1000)\ V/m$ over 1000 time step
- Magnetic field: $\mathbf{H} = 0\ A/m$ at $t = 0$

Results are shown in Figure 5.4. We observe that the effective properties decrease with temperature following the trend imposed by the variation of the properties of the particles. Then they become steady as the properties of the particle reach their constant threshold.

This model simulation shows the advantage of a particle doped composite over a raw material having decreasing properties with temperature. Indeed, making particles from this raw material and using them to manufacture a particle doped composite employing a matrix material with thermally independent properties would allow for higher electromagnetic properties at high temperature.

Also, it is possible to use such predictions to carry out coupled electromagnetic-thermal simulations over the actual macro composite material. Assuming effective thermal properties are known, one could now simultaneously solve Maxwell's equations and the heat equation while taking into account pointwise variations of the effective electromagnetic properties due to local temperature variations.

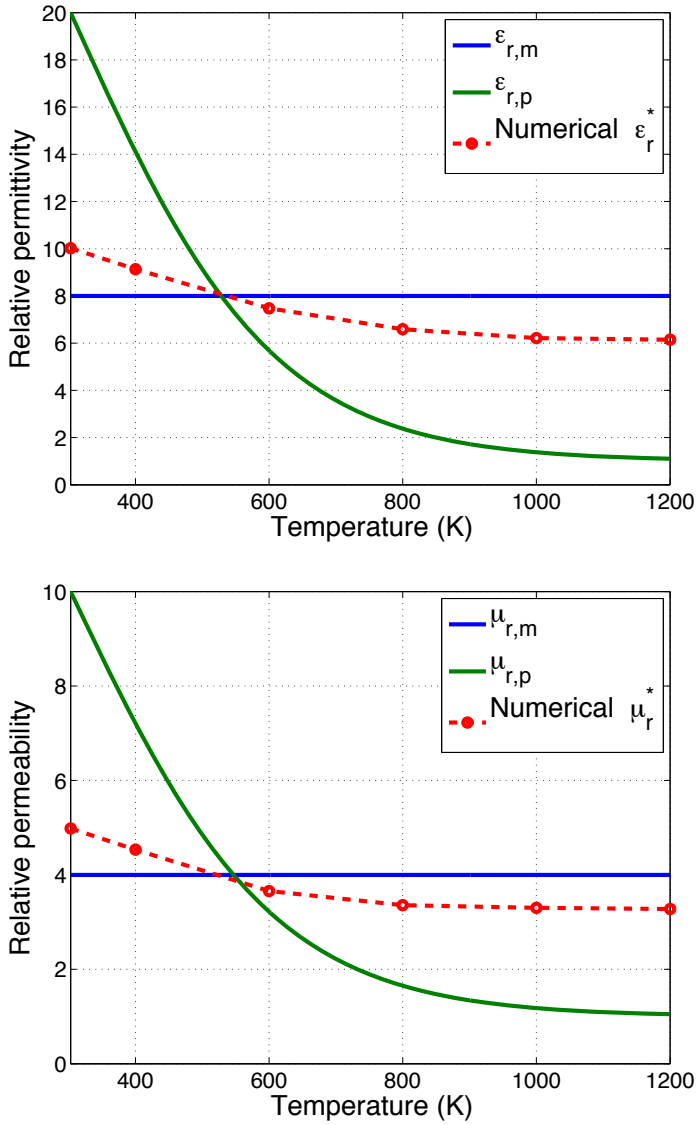

Figure 5.4: Evolution of relative effective electric permittivity ϵ_r^* (top) and relative effective magnetic permeability μ_r^* (bottom) as a function of temperature for the test problem.

Chapter 6

Numerical design of particle doped composite for electromagnetic applications

In this chapter we propose a numerical method that allows to answer the following question: "If I desire to manufacture a particle doped composite with effective electromagnetic properties ϵ_D^* and μ_D^*, what mixing parameters should I use?"

6.1 Motivation

In the previous sections we proposed a numerical method to estimate the effective electromagnetic properties of a particle doped composite with known mixing parameters. During the design process of such a composite, it is often the reverse problem that is encountered: the desired effective properties are known and we are to determine the appropriate mixing parameters for the composite to achieve these desired properties. The following parameters, identified previously as having influence on the effective electromagnetic properties, must be optimized:

- The electric permittivity of matrix material ϵ_m and particles ϵ_p
- The magnetic permeability of matrix material μ_m and particles μ_p
- The volume fraction of the particles v_p
- The diameter of the particles d

Any other parameters that may affect the effective properties are neglected in this study. Range restrictions may be specified on some or all of these parameters. Also, it is possible to fix some parameters, for instance the properties of the matrix material, in case such restrictions apply.

An optimization technique using Hashin-Shtrikman bounds has been developed in [32]. Following the same technique we present a method to optimize these parameters using the previously introduced numerical method to estimate effective electromagnetic properties instead of Hashin-Shtrikman bounds.

6.2 Numerical method

6.2.1 Test Function

A test function is to be introduced first. This is the function we want to optimize. Let $\lambda = (\epsilon_m, \epsilon_p, \mu_m, \mu_p, v_p, d)$ the vector of parameters to be optimized. Following [32] we introduce the test function

$$F(\lambda) = w_\epsilon \left| \frac{\epsilon^*(\lambda) - \epsilon_D^*}{\epsilon_D} \right| + w_\mu \left| \frac{\mu^*(\lambda) - \mu_D^*}{\mu_D} \right| \tag{6.1}$$

where ϵ_D^* and μ_D^* are the desired effective properties, and $\epsilon^*(\lambda)$ and $\mu^*(\lambda)$ are the terms we are trying to optimize in order to minimize F i.e. bring it as closer to zero as possible. The parameters w_ϵ and w_μ are positive weights that are adjusted depending on the importance of each of the effective properties.

A desired tolerance tol_D is often specified on the value of F such that the search for the optimizing λ is stopped when $F \leq tol_D$.

6.2.2 Genetic algorithm

We want to use the numerical method introduced in Chapter 4 to evaluate the effective properties $\epsilon^*(\lambda)$ and $\mu^*(\lambda)$ for λ. Due to the complexity brought on by the test function, it is decided to use the optimization technique known as genetic algorithm. It is a popular technique to optimize non-linear systems with large numbers of variables. We refer to [3] for a detailed explanation of the method and its various applications.

The method consists of generating a set of N_s random strings λ_i, called population. Then, they are plugged into the test function. The value F_i of the test function corresponding to λ_i is commonly designated as the fitness of λ_i. If one of the fitness meets the specified tolerance, we stop. Otherwise we repeat with N_s new random strings until tolerance is met. To accelerate the process the N_{top} top performing strings are often kept and each successive two top strings are linearly combined to produce "child" strings

$$\lambda_k^{\text{child } j} = \alpha_k \lambda_k^{\text{parents } i} + (1 - \alpha_k) \lambda_k^{\text{parents } i+1} \tag{6.2}$$

where the subscript k indicates the component of λ (for instance $k = 1$ designates ϵ_m), the superscript j designates the j^{th} child, and the superscript i designates the i^{th} top parent string. Here α_k is a random number between 0 and 1. In this case, the N_{top} parent strings and N_{child} children per couple are kept for the new population, and more strings are randomly generated to obtain a population of size N_s. Once again, the process is repeated until the convergence criterion is met. This is described properly in the flowchart given in the next section.

6.2.3 Flow chart

We give in Figure 6.1 a detailed flowchart of the numerical method proposed to optimize mixing parameters of a composite to achieve desired properties. Computation of effective properties for each string being an independent process, it is parallelized in the proposed method.

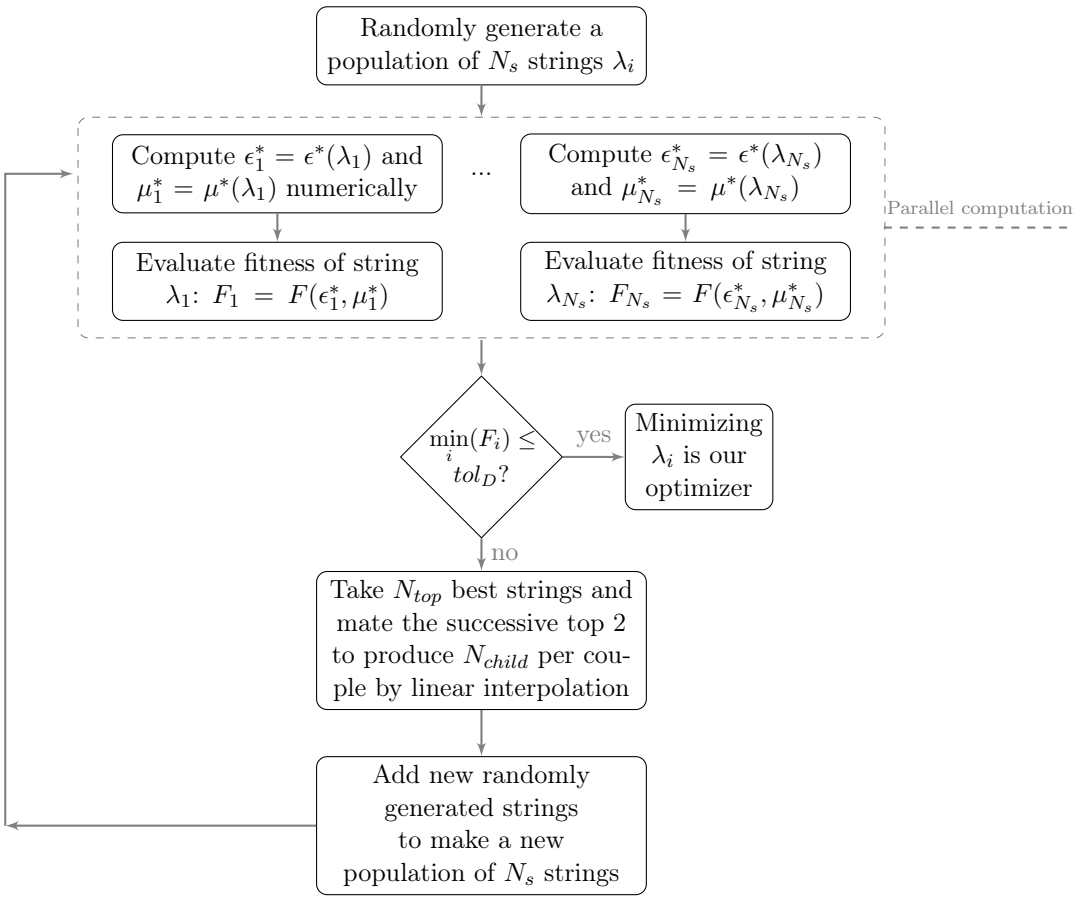

Figure 6.1: Flowchart of the overall numerical method proposed to estimate the effective electromagnetic properties.

6.3 Results on a test simulation

The method is applied to a test problem. We assume that the properties of the matrix material are known. We are looking for the appropriate particle material properties $\epsilon_{r,p}$ and $\mu_{r,p}$, its quantity v_p and its diameter d to achieve desired effective electric permittivity ϵ^*.

The following parameters are used

1. Matrix material properties
   - Relative electric permittivity: $\epsilon_{r,m} = 1$
   - Relative magnetic permeability: $\mu_{r,m} = 1$
2. Desired properties
   - Relative effective electric permittivity: $\epsilon^*_{r,D} = 10$
3. Genetic algorithm parameters
   - $N_s = 20$
   - $N_{top} = 4$
   - $N_{child} = 2$
   - Tolerance on fitness $tol_D = 2 \times 10^{-4}$
   - Range on relative electric permittivity of particle: $50 \leq \epsilon_{r,p} \leq 400$
   - Range on relative magnetic permeability of particle: $40 \leq \mu_{r,p} \leq 200$
   - Range on particle volume fraction: $0.05 \leq v_p \leq 0.2$
   - Range on particle diameter: $2\mu m \leq d \leq 10\mu m$
   - Weights: $w_\epsilon = 1$, $w_\mu = 0$
4. Numerical solver parameters
   - Mesh size $\Delta x = \Delta y = \Delta z = \frac{d}{10}$
   - $\Delta t = \Delta t_{CFL}$
5. Electromagnetic field
   - Electric field: $\mathbf{E} = (0, 0, 0)\ V/m$ at $t = 0$ and linearly growing with time on the side of the RVE with normal $\mathbf{e}_y$ and $-\mathbf{e}_y$ until $\mathbf{E} = (1000, 1000, 1000)\ V/m$ over 1000 time step
   - Magnetic field: $\mathbf{H} = 0\ A/m$ at $t = 0$

The results are shown next. We show in Figure 6.2 the fitness of best performing string per population. We see that the tolerance is reached after 58 populations (although we let the code run for 70 populations). The evolution of the parameters for the best performing string per population is shown in Figure 6.3. Finally Table 6.1 lists the top 5 strings from the final population along with their fitness.

The parameters suggested by the method are obviously not realistic. For instance, a material with suggested ϵ_r and μ_r might not exist. However, the method provides a target range for these parameters. A post processing work is still required to determine any existing material with characteristics closest to the one specified by this method. A final numerical evaluation of effective electromagnetic properties with the material selected would be required to check that the desired effective electromagnetic properties are indeed achieved.

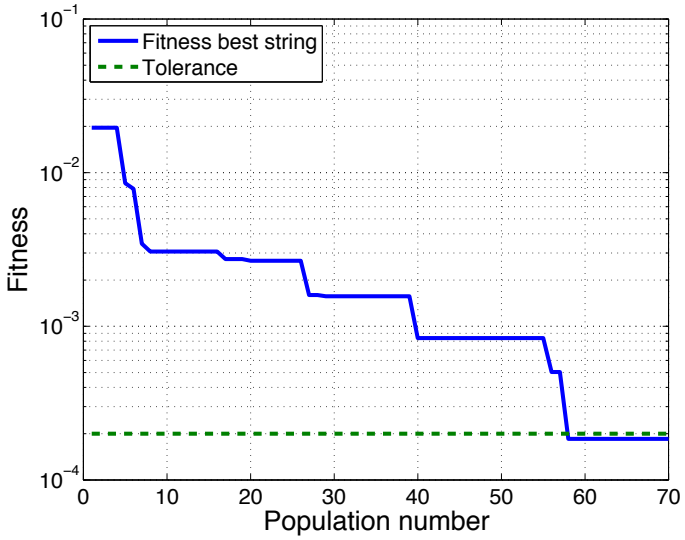

Figure 6.2: Evolution of the fitness for the best performing string per population. Tolerance for the fitness is met with population number 58.

String number	$\epsilon_{r,p}$	$\mu_{r,p}$	v_p	d (μm)	ϵ_r^*	Fitness (10^{-4})
1	235.8586	127.8108	0.14555	3.3301	10.0018	1.8521
2	238.3521	127.5618	0.1456	3.3302	9.9980	1.9599
3	238.6493	127.5157	0.1456	3.3321	10.0050	5.0412
4	234.9355	128.2741	0.14554	3.3251	10.0083	8.3800
5	237.08350	127.7310	0.14555	3.3301	10.14577	145.7823

Table 6.1: Parameters from the top 5 best performing string from the final population.

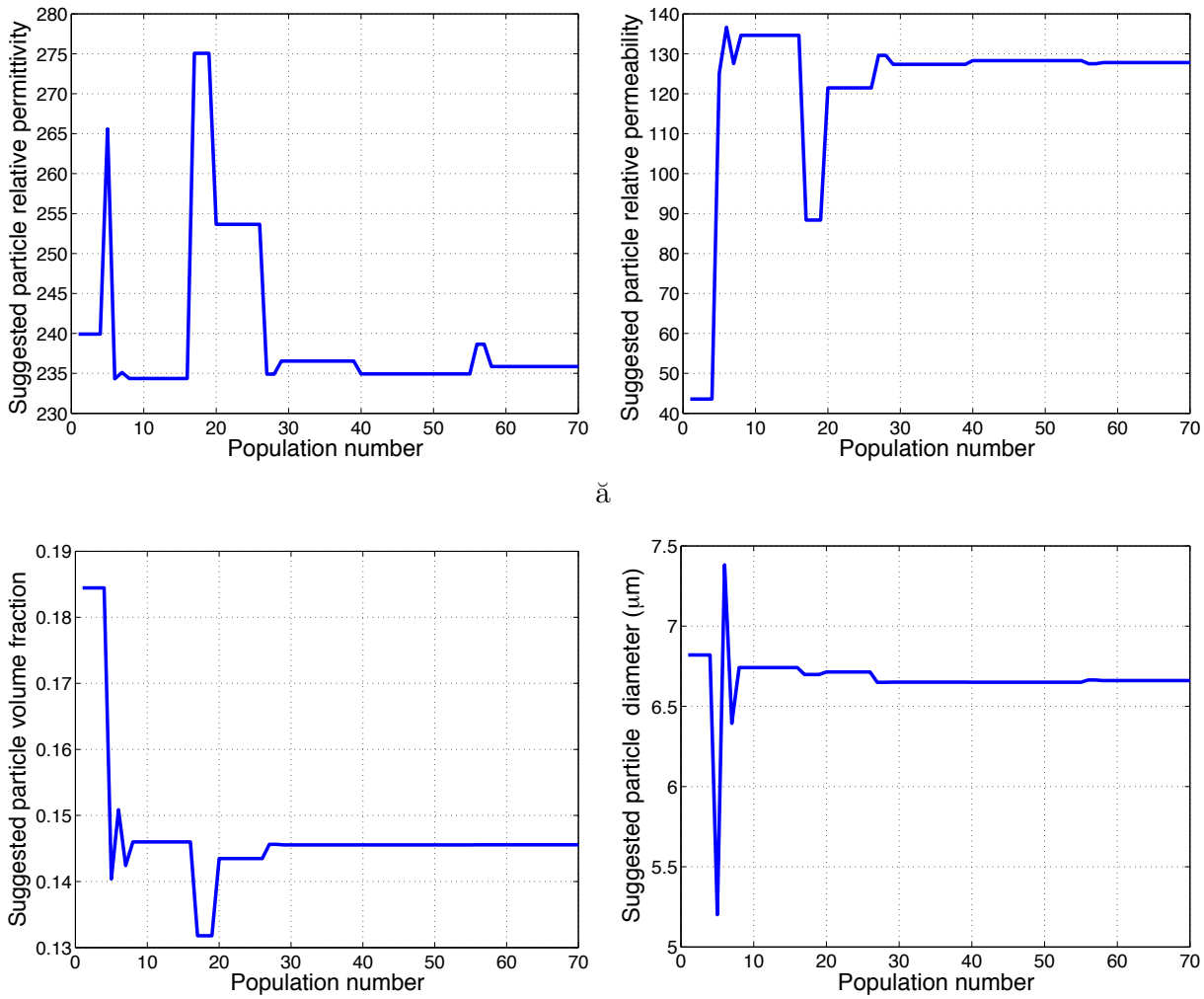

ă

Figure 6.3: Evolution of the suggested parameters by the best performing string per population.

Chapter 7

Closing comments

Driven by applications to electromagnetic components of MEMS, the focus of this work was on estimating the effective electromagnetic properties of particle doped composites.

After reviewing the theory of electromagnetism, the concept of homogenization and effective properties were introduced. Some popular analytical bounds for the effective electric permittivity and effective magnetic permeability were presented. Observing their limitations, a numerical method to estimate these effective properties was proposed.

A numerical method using Yee's scheme to solve dynamic Maxwell's equations was developed. The method was applied to a test problem and numerical results were validated with analytical bounds. The results were also compared to some experimental data available. A noticeable difference was observed. The main source of error was identified as being the incapacity of the numerical method to capture exactly the spherical shape of the particles. Improved numerical scheme able to capture special features could be implemented to improve the accuracy of the results. Still, a better performance than the analytical bounds available was shown by the numerical method. The capacity of the method to work for various shapes of particle has also been shown.

The model was then extended to predict the thermal variation of the effective properties. The results could be used to conduct coupled EM-thermo simulation by solving simultaneously Maxwell's equations and the heat equation on the actual macro composite using effective properties (assuming effective thermal properties are known). One could then track the point wise variation of effective electromagnetic properties due to local change in temperature.

Finally a numerical optimization method was introduced to estimate optimal parameters for a particle doped composite to achieve desired effective electromagnetic properties. The method combined genetic algorithm with the numerical method previously proposed to estimate effective electromagnetic properties. The scheme showed good performance on a test

problem.

Considerations for future work mainly include implementation of an improved scheme for Maxwell's equations to capture exactly the spherical shape of the particles.

Bibliography

[1] J Anderson, M Okoniewski, and SS Stuchly. Practical 3-d contour/staircase treatment of metals in fdtd. *Microwave and Guided Wave Letters, IEEE*, 6(3):146–148, 1996.

[2] Deborah DL Chung. *Composite materials: functional materials for modern technologies*. Springer Science & Business Media, 2003.

[3] Lawrence Davis et al. *Handbook of genetic algorithms*, volume 115. Van Nostrand Reinhold New York, 1991.

[4] KH Dridi, Jan S Hesthaven, and Adi Ditkowski. Staircase-free finite-difference time-domain formulation for general materials in complex geometries. *Antennas and Propagation, IEEE Transactions on*, 49(5):749–756, 2001.

[5] WJ Drugan and JR Willis. A micromechanics-based nonlocal constitutive equation and estimates of representative volume element size for elastic composites. *Journal of the Mechanics and Physics of Solids*, 44(4):497–524, 1996.

[6] Reza Ghodssi and Pinyen Lin. *MEMS materials and processes handbook*, volume 1. Springer, 2011.

[7] David J Griffiths. *Introduction to electrodynamics*. Pearson, 2013.

[8] Jon Häggblad and Olof Runborg. Accuracy of staircase approximations in finite-difference methods for wave propagation. *Numerische Mathematik*, 128(4):741–771, 2014.

[9] Zvi Hashin and Shmuel Shtrikman. A variational approach to the theory of the effective magnetic permeability of multiphase materials. *Journal of applied Physics*, 33(10):3125–3131, 1962.

[10] Henry W Haslach Jr. Electromagnetism and joule heating. In *Maximum Dissipation Non-Equilibrium Thermodynamics and its Geometric Structure*, pages 257–268. Springer, 2011.

[11] Rm Hill. The elastic behaviour of a crystalline aggregate. *Proceedings of the Physical Society. Section A*, 65(5):349, 1952.

[12] Derek Hull and TW Clyne. *An introduction to composite materials*. Cambridge university press, 1996.

[13] J. D. Jackson. *Classical Electrodynamics*. Wiley, third edition, 1998.

[14] Attay Kovetz. *Electromagnetic theory*. Oxford University Press Oxford, 2000.

[15] James Clerk Maxwell. *A treatise on electricity and magnetism*, volume 1. Clarendon press, 1881.

[16] Hari Singh Nalwa. *Handbook of Low and High Dielectric Constant Materials and Their Applications, Two-Volume Set*. Academic Press, 1999.

[17] M Lj Napijalo, Z Nikolić, J DojčIloviĆ, MM Napijalo, and L Novaković. Temperature dependence of electric permittivity of linear dielectrics with ionic and polar covalent bonds. *Journal of Physics and Chemistry of Solids*, 59(8):1255–1258, 1998.

[18] P Markondeya Raj, Prathap Muthana, T Danny Xiao, Lixi Wan, Devarajan Balaraman, Isaac Robin Abothu, Swapan Bhattacharya, Madhavan Swaminathan, and Rao Tummala. Magnetic nanocomposites for organic compatible miniaturized antennas and inductors. In *Advanced Packaging Materials: Processes, Properties and Interfaces, 2005. Proceedings. International Symposium on*, pages 272–275. IEEE, 2005.

[19] Thomas Rylander, Pär Ingelström, and Anders Bondeson. *Computational electromagnetics*, volume 51. Springer Science & Business Media, 2012.

[20] K Sab. On the homogenization and the simulation of random materials. *European journal of mechanics. A. Solids*, 11(5):585–607, 1992.

[21] Dinker B Sirdeshmukh, Lalitha Sirdeshmukh, and KG Subhadra. *Micro-and Macro-properties of Solids*. Springer, 2006.

[22] Shigeyuki Somiya. *Handbook of Advanced Ceramics: Materials, Applications, Processing, and Properties*. Academic Press, 2013.

[23] G.P. Srivastava and Y.P. Varshni. Variation of dielectric constant with temperature. *Physica*, 22(6-12):584–586, 1956.

[24] A Brent Strong. *Fundamentals of composites manufacturing: materials, methods and applications*. Society of Manufacturing engineers, 2008.

[25] A. Taflove and S. C. Hagness. *Computational electrodynamics*, volume 160. Artech house Boston, 2000.

[26] Manabu Takeuchi. An experimental study on the effective dielectric constant of heterogeneous media. In *Properties and Applications of Dielectric Materials, 1991., Proceedings of the 3rd International Conference on*, pages 1064–1067. IEEE, 1991.

[27] Anju Toor, Jim C Cheng, and Albert P Pisano. Synthesis and characterization of gold nanoparticle/su-8 polymer based nanocomposite, 2014.

[28] Salvatore Torquato. *Random heterogeneous materials: microstructure and macroscopic properties*, volume 16. Springer Science & Business Media, 2002.

[29] O. Wiener. Zur theorie der refraktionskonstanten. berichte uber die verhandlungen der koniglich-sachsischen gesellschaft der wissenshaften zu leipzig. *Math.-Phys. Klasses*, 62:256–277, 1910.

[30] C. Yang, K. Koh, X. Zhu, and L. Lin. On-chip rf inductors with magnetic nano particles medium. pages 2801–2804, 2011.

[31] Kane S Yee. Numerical solution of initial boundary value problems involving maxwell's equations. *IEEE Trans. Antennas Propag*, 14(3):302–307, 1966.

[32] Tarek I Zohdi. *Electromagnetic properties of multiphase dielectrics: a primer on modeling, theory and computation*, volume 64. Springer Science & Business Media, 2012.

[33] Tarek I Zohdi and Peter Wriggers. *An introduction to computational micromechanics*. Springer Science & Business Media, 2008.

[34] TI Zohdi. An adaptive-recursive staggering strategy for simulating multifield coupled processes in microheterogeneous solids. *International journal for numerical methods in engineering*, 53(7):1511–1532, 2002.